R. & M. No. 3800

R. & M. No. 3800

PROCUREMENT EXECUTIVE, MINISTRY OF DEFENCE

AERONAUTICAL RESEARCH COUNCIL

REPORTS AND MEMORANDA

Calculations of the Effects of Blowing from the Leading Edges of a Cambered Delta Wing

By J. E. BARSBY

University of Liverpool

LONDON: HER MAJESTY'S STATIONERY OFFICE

1978

£5·25 net

Calculations of the Effects of Blowing from the Leading Edges of a Cambered Delta Wing

By J. E. BARSBY

University of Liverpool

Reports and Memoranda No. 3800*

September, 1975

Summary

The thin jet model applied by Spence to the study of the jet flap is combined with the vortex sheet model applied by Mangler and Smith to the study of leading-edge separation, to study the effect of blowing from the leading-edges of a cambered wing. The numerical techniques used to solve problems of leading-edge separation have been improved, and in the present investigation solutions have been generated for various values of the lift, camber and blowing strength of the jet whose direction is restricted to lie in a plane normal to the free stream. Regions existed in the parameter space within which solutions could not be obtained and there were regions within which solutions were not unique. The downward deflection of the jet which is associated with the camber does not produce a lift increment due to blowing which is significantly larger than the increment produced by the same blowing momentum on a plane wing. However, the drag for a given lift when blowing is introduced is greatly reduced, and in some cases a negative drag is predicted.

* Replaces A.R.C. 36 252

LIST OF CONTENTS

1. Introduction

The low pressure areas which are induced over the wing surface due to the complicated flow in the cores of the leading-edge vortex system which is formed when a slender delta wing is placed at incidence to a uniform stream can contribute an appreciable amount to the lift. By introducing a thin jet blowing air out from the leading edge of the wing the strength of these leading edge vortices can be increased. A theoretical investigation by Barsby[1] on the effects of such a jet introduced along the leading edges of a flat plate delta wing suggests that substantial lift increments can be obtained for a given jet strength, the maximum increments occurring when the jet direction is normal to the leading edge. Furthermore when the effects of the trailing edge are taken into account the results obtained show reasonable agreement with the experimental work of Alexander[2] and Trebble[3]. The direction of the jet is assumed to be in the plane of the wing and although the lift created by the wing is increased, since the momentum flux of the jet enhances the vortex strength, no advantage is gained from the reaction of the jet on the wing. By angling the jet direction downwards it is possible to obtain increases in the lift by both increasing the strength of the leading-edge vortices and incorporating a direct thrust from the jet. In this paper the effects of blowing from a conically cambered delta wing are considered where the cross-section of the wing is an arc of a circle. The direction of the jet along each leading edge is taken to lie in the tangent plane of the wing surface at the leading edge. Theoretical investigations have been carried out on such wings without blowing for attached flow by Smith[4] and for separated flows by Barsby[5] and Squire[6].

The model adopted to represent the three-dimensional separated flow is derived from that used by Smith[7] in his treatment of the flow past a flat plate delta wing at incidence to a uniform stream. The effects of the jet are incorporated into the model by using the thin jet flap approximation of Spence[8]. The method adopted to solve the resulting integro-differential equations is that developed by Barsby[9].

1.1. Assumptions

As shown in Fig. 1 we consider a conically cambered slender delta wing placed at incidence to a uniform stream. The assumptions which we make are similar to those made in Ref. 1 and a detailed description of their validity and significance can be found in Refs. 1 and 7. These assumptions are,

(i) The effect of viscosity is neglected.

(ii) All the vorticity in the fluid is condensed into two vortex sheets. These vortex sheets originate from each leading edge of the wing and roll up to form two spiral vortex cores. The central regions of these two vortex spirals are replaced by isolated line vortices, a cut is required between each line vortex and the end of its associated vortex sheet to render the flow variables single-valued.

(iii) The flow is assumed to be conical.

(iv) The slender body theory of Munk, Jones, and Ward is appropriate.

(v) The effects of the jet are considered in the limit as the width of the jet tends to zero with the momentum flux maintained at a constant value as in Refs. 1 and 8.

The effect of assumptions (i) and (ii) is to allow the flow, away from the singular lines and surfaces, to be calculated in terms of a potential function. Assumption (iii) reduces the number of independent variables from three to two. Assumption (v) allows us to simplify the jet flow in the following way. Assume that the jet is separated from the main flow by two vortex sheets, distance δ_J apart. Let ρ_J be the density and V_J the speed of the jet fluid, then by assuming the jet to be inviscid and irrotational it can be shown that the pressure difference across the jet at any point is proportional to the product of the momentum flux $J = \delta_J \rho_J V_J^2$ and the curvature of jet streamline at that point. The limit of zero jet thickness effectively reduces the jet of air to a singular stream surface and since this surface originates from the leading edge it combines with the vortex sheet to form a so-called jet-vortex sheet, which differs from a vortex sheet only in the respect that it can sustain a pressure jump. Barsby[1] shows that the effects of the jet only extend a finite distance along the spiral vortex sheet, and that if this distance exceeds the length of the truncated vortex sheet then some account must be taken of the pressure jump sustained by that part of the jet. This is most easily achieved by integrating the pressure jump along that part of the jet which extends past the finite vortex sheet and representing the integral as a force sustained by the isolated vortex and cut. The effects of this force on the structure of the vortex system is small and although the evaluation of this force by Barsby[1] was later found to be incorrect the effect on the results was negligible.

The effect of the assumptions outlined above is to reduce the problem to solving Laplace's equation in two dimensions subject to boundary conditions on the wing, at infinity, on the finite jet-vortex sheets, and on the isolated line vortices and cuts. A Kutta condition is applied at the leading edge to ensure that the fluid velocities remain finite along the leading edges of the wing.

1.2. Solution Procedure

The assumptions outlined in the previous section reduce the problem to one of solving Laplace's equation in two dimensions. By choosing a suitable non-dimensional form for the two independent variables we can satisfy the eyuation by construtıng an analytic function for the complex potential. The wing boundary conditions and the conditions at infinity depend solely upon the incidence and shape of the wing. Smith[4] has calculated a complex potential function for such a wing where the flow remains attached. Barsby[5], by using certain conformal transformations, was able to combine Smith's function with contributions from the vortex sheet and isolated vortex so that the conditions on the wing and at infinity remained satisfied. The introduction of leading edge blowing requires no further modification to this complex potential function.

The shape and strength of the jet-vortex and the position and strength of the isolated vortex are determined by applying conditions along the jet-vortex sheet, a condition at the isolated vortex, and a Kutta condition at the leading edge. The jet-vortex sheet sustains a pressure jump, which is a function of its shape, and must form a stream surface in the three-dimensional flow. The combined vortex and cut sustains a force equal to the integral of the pressure jump across that point of the jet sheet which extends past the finite jet-vortex sheet. Finally, a Kutta condition is applied at the leading edge to ensure the flow remains finite at that point.

These conditions can be recast as a set of m simultaneous non-linear equations in m unknowns by using the numerical discretisation techniques described in the Appendix. Solutions to these equations are then calculated using an m-dimensional form of Newton's method. Successive iterates are generated until a solution is found for a particular value of the lift with the blowing rate and the wing camber fixed.

1.3. Summary of Results

The methods just described yield solutions dependent upon five parameters; incidence, camber, blowing strength, blowing angle and wing semi-apex angle. By choosing a jet direction perpendicular to the free stream the number of independent parameters considered can be reduced to three; incidence, camber and blowing strength. Solutions were successively computed for various cambers and jet strengths varying the incidence until solutions were obtained for particular values of the lift.

Solutions could not be generated for high camber parameters and there were regions in the parameter space in which the solutions found were not unique. These regions contained the particular values of the incidence and camber for which the flow remains attached in the no blowing case.

Lift increments produced by angling the jet downwards do not significantly exceed those calculated for a flat plate delta wing. However, it is found that leading-edge blowing is effective if it is desired to increase the lift while keeping the incidence fixed. An approximate expression has been calculated which summarises the relation between the drag and lift, camber, and blowing parameters. From this expression the effect of combining leading-edge blowing with camber can be seen. To reduce the drag for a given lift the expression suggests that higher camber parameters than those considered here may be of interest.

2. Mathematical Treatment

2.1. Equations governing the Flow Field

With reference to Fig. 1 we introduce a right-handed coordinate system $Oxyz$. The origin O is at the apex of the wing which is assumed to have a circular arc section, the x-axis lies along the projection of the wing centre line in the plane of the leading edges, the z-axis lies in a direction normal to this plane and the y-axis lies to starboard. The projection of the wing in the xy-plane is a plane delta with semi-apex angle γ. The centre line of this projection is at an angle α to the uniform stream. If the local semi-span of this projection is of length $s = x \tan \gamma$, then the camber of the wing can be expressed in terms of a parameter p where ps is the local height of the wing centre line above the x-axis. A local value is interpreted as the value in a particular cross-flow plane, i.e. a plane in which $x =$ constant. The equation for the wing surface may then be written as

$$y^2+\left(z+\frac{1-p^2}{2p}x \tan \gamma\right)^2-\left(\frac{q^2}{2p}x \tan \gamma\right)^2=0, \tag{1}$$

where $-s \leq y \leq s$, $q=(1+p^2)^{\frac{1}{2}}$. The case $p=0$ corresponds to a flat plate delta wing.

The incidence α and the semi-apex angle γ are assumed to be small, and an incidence parameter is defined as $a = \alpha \tan \gamma = O(1)$. If the velocity of the fluid $\mathbf{V}$ is written in terms of a disturbance potential Φ, we have

$$\mathbf{V} = \nabla(Ux + \Phi), \tag{2}$$

where U is the speed of the undisturbed flow.

The assumptions outlined in Section 1 reduce the problem to one of solving the following two-dimensional Laplace equation in the cross-flow plane,

$$\Phi_{yy} + \Phi_{zz} = 0 \tag{3}$$

Conditions must be satisfied on the wing, at infinity, on the jet-vortex sheets, on the isolated line vortices and cuts, and at the leading edges. We now introduce a non-dimensional complex potential W as

$$W = (\Phi + i\Psi)/Us \tan \gamma, \tag{4}$$

where W is a function of the complex representation of the cross-flow plane

$$Z = (y + iz)/s. \tag{5}$$

To solve equation (3) we must construct an analytic form for W which satisfies all the boundary conditions. Once W is known for a particular cross-flow plane the assumption of conical flow ensures that W is known for the whole flow field.

2.2. Boundary Conditions on the Jet-Vortex Sheet

In an inviscid flow vorticity is convected with the fluid, and the first condition to be applied is that the jet-vortex sheet must be a stream surface in the three-dimensional flow.

In Fig. 2 the coordinate representation of the intersection of the jet-vortex sheet with the cross-flow plane is shown. The arc length measured along the sheet from the leading edge B to a point C is denoted by σs. The polar coordinates of the sheet about the origin A of the cross-flow plane are denoted by rs and θ. The angle of the tangent the sheet at C with the line AB is denoted by ψ and $\mathbf{n}$ represents the normal to the sheet. The condition that the jet-vortex sheet forms part of a stream surface can be written as

$$\frac{\Phi_n}{Us \tan \gamma} = -r \sin \phi, \tag{6}$$

and is the condition derived by Smith[7].

The three-dimensional jet-vortex sheet is a developable surface and can be 'unrolled' into a plane surface without stretching so that distances along particular lines in the surface remain unchanged. Maskell[10] has pointed out that in an inviscid fluid the fluid particles in a thin jet will only experience a force due to the pressure difference across the jet. Consequently the direction of acceleration of these particles, which lies along the principal normal to the path which they follow, must also lie along the surface normal of the sheet. The condition that these two normals coincide is a condition which implies that the path of a particle in the jet lies along a geodesic in the surface. When the sheet is 'unrolled' into a plane surface these geodesics become straight lines. Since the jet-vortex sheet joins the wing surface smoothly, the tangent planes of the wing surface and of the jet-vortex sheet are coincident along the leading edge. The direction of the jet must lie in this plane and we assume that it is at an angle β to the leading edge. In Fig. 3 we show the 'unrolled' jet-vortex sheet together with the projected wing surface in the xy-plane. Since the angle β is measured in a tangent plane of the jet-vortex sheet, its value remains unchanged by the transformation. The definition of the angle β differs from the definition used by Barsby[1].

From Spence's jet flap theory we know that the pressure jump sustained by the jet sheet can be calculated as a function of its shape, and is proportional to the strength of the jet and the curvature of the jet streamline. A condition to be satisfied on the jet-vortex sheet is then formulated by ensuring that this pressure jump is equal to the pressure jump across the sheet as calculated from the flow field. If the pressure jump sustained by this sheet as calculated by the jet-flap theory of Spence[8] is ΔC_p, where Δ is the difference operator across the sheet (inside minus outside), then the condition that the pressure difference as predicted by the flow field is equal to ΔC_p is given below and is the equation derived by Barsby[1],

$$\frac{\Delta\Phi}{Us\tan\gamma}=\frac{\Delta\Phi_\sigma}{Us\tan\gamma}\left(r\cos\phi-\frac{\Phi_{\sigma M}}{Us\tan\gamma}\right)+\frac{1}{2}G \tag{7}$$

where

$$G=-\Delta C_p/\tan^2\gamma \tag{8}$$

In the case when there is no blowing the force sustained by the combination of the isolated line vortex and the cut is zero. However in the present case if the effect of the jet extends past the end of the truncated sheet then there remains an unbalanced pressure jump in the flow field. By integrating this pressure jump along that part of the jet sheet that extends past the end of the finite vortex sheet we obtain a force. This force must be sustained by the combined vortex and cut. We can also see from Fig. 3 that the jet sheet itself can only extend a finite distance along the trace of the vortex sheet in the cross-flow plane. This is shown by the limiting streamline OM. If σ_E is the arc length of the finite jet-vortex sheet and σ_M the arc length of the jet sheet, then we have the following expression for that force

$$f=s\int_{\sigma_E}^{\sigma_M}\tfrac{1}{2}\rho U^2\Delta C_p\,e^{i(\psi-\frac{1}{2}\pi)}\,d\sigma \tag{9}$$

where f is a force per unit length of the wing. The force on the combination of vortex and cut due to the flow field has been calculated by Smith[7] as

$$i\rho U^2\tan^2\gamma s\Gamma(Z_V-Z_E)-i\rho U^2\tan^2\gamma s\Gamma\left(-Z_V+\overline{\lim_{Z\to Z_V}\left(\frac{dW}{dZ}-\frac{\Gamma}{2\pi i}\frac{1}{Z-Z_V}\right)}\right) \tag{10}$$

where an overbar denotes the complex conjugate, Z_V and Z_E are the complex coordinate of the isolated vortex and the end of the finite vortex sheet respectively, and Γ is the strength of the isolated line vortex. Equating expressions (9) and (10) and setting $F=f/\frac{1}{2}\rho U^2 s\tan^2\gamma$ we have the following equation for the force condition on the isolated vortex and cut,

$$0=(2\bar{Z}_V-\bar{Z}_E)-\lim_{Z\to Z_V}\left(\frac{dW}{dZ}-\frac{\Gamma}{2\pi i}\frac{1}{Z-Z_V}\right)-\frac{i\bar{F}}{2\Gamma} \tag{11}$$

We must now calculate expressions for G and F in terms of the shape of the sheet. In Fig. 3 DC is an 'unrolled' jet streamline and the value of the angle BDC is β. Let the semi-span of the wing in a particular cross-flow plane be s, and let s_0 be the semi-span in the plane in which the jet streamline DC originates. A simple geometrical argument yields the following relation

$$\frac{su}{\sin\beta}=\frac{s_0\operatorname{cosec}\gamma}{\sin(\beta-v)} \tag{12}$$

where su is the length OC and v the angle BOC. By considering the sheet in its original form as shown in Fig. 2 and using the fact that distances measured along the sheet surface remain unchanged by the unrolling of the sheet, we can deduce that

$$\begin{aligned}u^2&=\cot^2\gamma+r^2,\\1&=u^2\left(\frac{dv}{d\sigma}\right)^2+\left(\frac{du}{d\sigma}\right)^2.\end{aligned} \tag{13}$$

If a point P on the sheet surface is denoted by $\mathbf{S}$ then $\mathbf{S}$ can be considered to be a function of s and σ, the semi-span of the wing in the cross-flow plane containing P and the arc length along the trace of the sheet in this cross-flow plane respectively. We have, therefore, $\mathbf{S}=\mathbf{S}(s,\sigma)$ and a line in this surface can be expressed in the following way

$$\mathbf{S}(s(\tilde{t}), \sigma(\tilde{t})) = s(\cot\gamma\, i + I_1 j + I_2 k) \tag{14}$$

where $\tilde{t}$ is a parameter which varies along the arc and I_1, I_2 are the integrals

$$I_1 = \int_0^{\tilde{t}} \cos\psi(\tilde{t}) \frac{d\sigma}{d\tilde{t}} d\tilde{t}, \qquad I_2 = \int_0^{\tilde{t}} \sin\psi(\tilde{t}) \frac{d\sigma}{d\tilde{t}} d\tilde{t} \tag{15}$$

Following the analysis of Barsby[1] we can apply the conditions for this line to be a geodesic to obtain the following equation for the curvature of the geodesic

$$\kappa = \frac{\left[\dfrac{\partial \mathbf{S}}{\partial s}, \dfrac{\partial \mathbf{S}}{\partial \sigma}, \dfrac{\partial^2 \mathbf{S}}{\partial \sigma^2}\right]\left(\dfrac{d\sigma}{d\tilde{t}}\right)^2}{\left|\dfrac{\partial \mathbf{S}}{\partial s} X \dfrac{\partial \mathbf{S}}{\partial \sigma}\right| \left|\dfrac{d\mathbf{S}}{d\tilde{t}}\right|^2} \tag{16}$$

where X denotes a vector product and [, ,] is a triple scalar product. If we now substitute equations (12)–(15) into equation (16) we obtain after some manipulation the following simplified expression for the geodesic curvature as in Barsby[1],

$$\kappa s_0 = \frac{\cos\gamma \sin^3(\beta - v)(\cot^2\gamma + I_1^2 + I_2^2)^{\frac{3}{2}}}{\sin\beta(\cot^2\gamma + (I_1 \sin\psi - I_2\cos\psi)^2)^{\frac{3}{2}}} \frac{d\psi}{d\sigma} \tag{17}$$

To obtain the value for G which is to be used in equation (7) we employ the jet-flap theory of Spence[8] outlined briefly in an earlier section. The pressure jump across sheet is proportional to the product of the momentum flux in the jet and the curvature of path of the particular jet particle passing through the point in question. In algebraic terms this may be expressed as

$$\Delta C_p = -\frac{\kappa J}{\frac{1}{2}\rho U^2}. \tag{18}$$

The momentum flux in the jet at a given point, J, remains constant along any jet streamline and is equal to its value at the initial point. In a conical theory the initial strength of the jet along the leading edge must vary in a conical manner which means that the strength of the jet streamline originating in the cross-flow plane with semi-span s_0 can be represented as follows,

$$J = M s_0 \quad \text{(per unit length of the leading edge)} \tag{19}$$

where M is a constant for a given blowing strength.

We define a blowing coefficient C_μ by referring the sum of the magnitudes of the momentum fluxes from both edges to the projected wing area and the free stream kinetic pressure, so that

$$C_\mu = \frac{2M\sin\beta}{\rho U^2 \cos\gamma}. \tag{20}$$

If we now assume that $C_\mu = 0(\gamma^2)$ and define a new parameter $c = C_\mu/\tan^2\gamma$ then

$$G = c\frac{d\psi}{d\sigma} \frac{\cos^2\gamma \sin^3(\beta - v)(\cot^2\gamma + I_1^2 + I_2^2)^{\frac{3}{2}}}{\sin^2\beta\,(\cot^2\gamma + (I_1\sin\psi - I_2\cos\psi)^2)^{\frac{3}{2}}}. \tag{21}$$

By integrating the pressure difference G from the end of the finite jet-vortex sheet to the point where the pressure difference falls to zero we obtain the following expression for the force F in equation (11)

$$F = i\int_{\sigma_E}^{\sigma_M} G(\sigma)\, e^{i\psi}\, d\sigma. \tag{22}$$

The expressions for G and F are cumbersome and can be simplified by adopting one of the assumptions of slender body theory, namely that the angle γ is small. If we assume $\gamma^2 \ll 1$ then the equations (13) yield the following simple equation

$$v = \gamma\sigma + O(\gamma^3). \tag{23}$$

Substituting this into equation (21) and eliminating terms $O(\gamma^2)$ we find

$$G = c\frac{d\psi}{d\sigma}(\sin\beta - 3\gamma\sigma\cos\beta) + O(\gamma^2). \tag{24}$$

In order to simplify the above expression for F, we introduce the variable $\zeta = \beta - \gamma\sigma$. Substituting equations (21) and (23) into (22) and eliminating terms of $O(\gamma^2)$, we obtain an expression for F containing the following integral,

$$I = i\int_{\xi_E}^{0} \sin^3\xi\, e^{i\psi}\frac{d\psi}{d\xi}\,d\xi. \tag{25}$$

Introducing a further variable χ by writing

$$\chi = \int_0^{\sigma_M} (Z - Z_V)\,d\sigma, \qquad \text{where } \chi = 0 \qquad \text{when } \sigma = 0 \tag{26}$$

we can evaluate the integral in expression (25), by parts, to obtain

$$I = -e^{i\psi_E}\sin^3\xi_E + 3\gamma(Z_V - Z_E)\sin^2\xi_E\cos\xi_E + 3\gamma^2 I_R \tag{27}$$

where

$$I_R = [\chi(2\sin\xi\cos^2\xi - \sin^3\xi]_{\xi_E}^{0} - \int_{\xi_E}^{0}\chi(2\cos^3\xi - 7\sin^2\xi\cos\xi)\,d\xi. \tag{28}$$

In order to prove that $I_R = 0(1)$ we have to show that χ is a bounded function of σ. For non-zero values of γ since $Z - Z_V$ is bounded then χ must also be bounded but as $\gamma \to 0$ $\sigma_M \to \infty$ and we have to show that $\lim_{\sigma_M \to \infty} \chi = \int_{\sigma_E}^{\infty}(Z - Z_V)\,d\sigma$ is bounded. Expressing $Z - Z_V$ in terms of polar coordinates $(\hat{r}, \hat{\theta})$ as $\hat{r}(\hat{\theta})\,e^{i\theta}$ about Z_V we find

$$\int (Z - Z_V)\,d\sigma = \int \left(\frac{d\hat{r}}{d\hat{\theta}} + \hat{r}^2\right)^{\frac{1}{2}} \hat{r}\, e^{i\hat{\theta}}\,d\hat{\theta}. \tag{29}$$

This last integral is bounded provided that $\hat{r}(\hat{\theta}) > \hat{r}(\hat{\theta} + 2\pi)$. Since the jet spirals inwards and cannot cross itself χ is bounded for all γ, and $I_R = 0(1)$. The resulting expression for F can be written as follows,

$$F = -c((\sin\beta - 3\gamma\sigma_E\cos\beta)\,e^{i\psi_E} + 3\gamma\cos\beta(Z_V - Z_E)). \tag{30}$$

2.3. Conditions on the Wing and at Infinity

The wing surface itself must be a stream surface of the three-dimensional flow, thus by substituting the equation for the wing surface (1) into the stream surface condition (6), we obtain the following condition at the wing,

$$\frac{\Phi_n}{Us\tan\gamma} = \frac{2p}{q^2}\left(1 - \frac{z}{s}\frac{1 - p^2}{2q}\right). \tag{31}$$

This condition is applied for $|y| \leq s$, $x =$ constant, and with z given by equation (1). A Kutta condition is applied at the leading edges of the wing and this condition can be written simply as

$$\frac{dW}{dZ} \quad \text{remains finite at } Z = \pm 1. \tag{32}$$

The condition to be satisfied at infinity may also be expressed in terms of the complex potential as

$$\frac{dW}{dZ}+ia\to 0 \qquad \text{as} \qquad Z\to\infty. \tag{33}$$

2.4. Construction of the Complex Potential

The construction of the complex potential follows that of Barsby[5] and is carried out in such a way as to satisfy the boundary conditions on the wing surface and at infinity automatically. By using a conformal transformation the trace of the wing surface in the cross-flow plane, the Z-plane is transformed into part of the imaginary axis in the new plane. The transformation and complex potential function constructed by Smith[4] are adequate when the flow remains attached. To model the separated flow, contributions from the transformed vortex system are added to the complex potential. The contributions are symmetrical about the wing in the transformed plane and the boundary conditions on the wing and at infinity remain satisfied.

The complete transformation consists of two conformal transformations. The first transforms the Z-plane into a ζ-plane and is given by

$$\zeta=\frac{Z-ip}{1-ipZ}. \tag{34}$$

In the ζ-plane the wing lies along part of the real axis. The point at infinity is transformed into the point $\zeta = i/p$. The second transformation transforms the ζ-plane into a Z^*-plane and is given by

$$Z^{*2}=\zeta^2-1. \tag{35}$$

In the Z^*-plane the wing becomes part of the imaginary axis, about which the flow is constrained to be symmetrical. The point at infinity in the cross-flow plane is transformed into the point $Z^*=iq/p$. In Fig. 4 a representation of the wing and vortex sheet can be seen in the Z^*-plane.

Although the complex potential is constructed in the Z^*-plane, it is the value of the arc length of the sheet measured in the cross-flow plane which is used as the independent variable. The position of the sheet in the Z-plane is represented by the function $Z(\sigma)$, and the strength of the sheet by the function $g(\sigma)$, where $g(\sigma)$ is given by

$$g(\sigma)=-\frac{1}{Us\tan\gamma}\frac{d\,\Delta\Phi}{d\sigma}. \tag{36}$$

The position of the sheet in the Z^*-plane can be calculated using equations (34) and (35). The strength of the isolated vortex is given by Γ and the position of the isolated vortex in the Z^*-plane is given by Z^*_V. The complex velocity in the Z^*-plane can now be constructed by placing the vortex system symmetrically about the imaginary axis, to give

$$\begin{aligned}\frac{dW}{dZ^*}=&\frac{ipq((3+p^2)\zeta+2qZ^*)}{2\zeta(q\zeta+Z^*)^2}-\frac{iaq}{(pZ^*-iq)^2}\\ &+\frac{\Gamma\mathcal{R}(Z^*_V)}{\pi i(Z^*-Z^*_V)(Z^*+\bar{Z}^*_V)}+\int_0^{\sigma_E}\frac{g(\sigma)\mathcal{R}(Z^*(\sigma))\,d\sigma}{\pi i(Z^*-Z^*(\sigma))(Z^*+\bar{Z}^*(\sigma))}.\end{aligned} \tag{37}$$

The first two terms in the above expression for dW/dZ^* are those derived by Smith[4] and satisfy the boundary conditions for the flow past the present wing configuration at the incidence for which the flow remains attached at leading edge. The last two terms are the contributions to dW/dZ^* from the isolated line vortices and finite jet-vortex sheets respectively. The velocity of the fluid in the Z-plane can be obtained by successively employing the following relations.

$$\frac{dW}{dZ}=\frac{dW}{dZ^*}\frac{dZ^*}{d\zeta}\frac{d\zeta}{dZ}$$

$$\frac{1}{U\tan\gamma}(\Phi_{\sigma_m}-i\Phi_n)=\frac{dW}{d\sigma}=\frac{dW}{dZ}\frac{dZ}{d\sigma}=e^{i\psi}\frac{dW}{dZ}. \tag{38}$$

3. Numerical Treatment

By taking Φ to be the real part of an analytic function W, we automatically satisfy Laplace's equation (3). By choosing the particular form for dW/dZ^* as given in equation (37), we satisfy the boundary conditions on the wing and at infinity. We have, as yet, to satisfy the velocity condition (6) and the pressure condition (7) on the finite jet-vortex sheet, the force condition (11) on the isolated vortex, and the Kutta condition (32) at the leading edges. The shape, $Z(\sigma)$, and strength $g(\sigma)$, of the sheet and the position, Z_V and strength Γ of the isolated vortex are now determined by satisfying these remaining conditions. A numerical procedure is adopted to solve these equations and suitable functions, from which the strength and shape of the sheet can be calculated, are chosen for the discretisation process in which the integro-differential equations are recast as simultaneous algebraic equations.

3.1. The Shape and Strength of the Jet-Vortex Sheet

The intrinsic coordinates ψ and σ are used to represent the shape of the finite jet-vortex sheet. Unfortunately the use of σ as the independent variable causes the integral in the complex potential to become an improper integral at the leading edge, $\sigma = 0$, and although it exists it cannot be calculated numerically. This problem may be overcome by defining σ in terms of a new parameter t such that $d\sigma/dt = 0$ at the point at which the integrand becomes infinite thus eliminating the singularity. The choice

$$\sigma(t) = \frac{kt^2(7-t)}{6(1+t)} \tag{39}$$

has the required property that $\sigma \sim t^2$ as $t \to 0$, and the advantage that $d\sigma/dt$ remains constant for values of t not too close to zero. In the present case t varied over the range $0 \leq t \leq 2{\cdot}4$ in steps of $0{\cdot}1$. By choosing suitable values for the parameter k the length of the finite part of the jet-vortex may be varied. With t as the independent variable the shape and strength of the sheet can be determined from the dependent variables $\psi(t)$ and $g(t)$. The coordinates of the sheet in the cross-flow plane are determined from the following equation

$$Z(t) = \int_0^t e^{i\psi(t)} \frac{d\sigma}{dt}\, dt. \tag{40}$$

3.2. Evaluation of the Cauchy Principal Value Integral

When $Z^* = Z^*(t)$ for some t the integral in equation (37) becomes an improper integral and it is interpreted as a Cauchy Principal Value Integral. Thus the evaluation procedure of the integral depends on the value of $Z^*$and the following methods are used to determine its value. If S denotes πi times the integral in question then

$$S = \int_0^{t_E} \frac{g(t)\mathcal{R}(Z^*(t))}{(Z^*-Z^*(t))(Z^*+\bar{Z}^*(t))} \frac{d\sigma}{dt}\, dt. \tag{41}$$

(i) For $Z^* \neq 0$ and Z^* not on the sheet, S is evaluated numerically using Simpson's rule.
(ii) For $Z^* = 0$ we have the following expression for S

$$S = -\int_0^{t_E} \frac{g(t)\mathcal{R}(Z^*(t))}{Z^*(t)\bar{Z}^*(t)} \frac{d\sigma}{dt}\, dt. \tag{42}$$

Again we can use Simpson's rule but we have to provide a value for the integrand at $t = 0$. After taking a series of limits as $z \to 0$ we find that

$$\lim_{t\to 0}\left[\frac{g(t)\mathcal{R}(Z^*(t))}{Z^*(t)\bar{Z}^*(t)} \frac{d\sigma}{dt}\right] = \left[\frac{-1}{Us\tan\gamma} \frac{d\,\Delta\Phi}{d\sigma}\right]_{\sigma=0} \left(\frac{7k}{3}\right)^{\frac{1}{2}} \tag{43}$$

and the value of this expression can be determined numerically from its value at neighbouring points along the sheet.

(iii) For $Z^* = Z_o^* \neq 0$, where Z_o^* is a point on the sheet we have to evaluate a Cauchy Principal Value Integral. This can be done by rearranging the integrand so that the singularity appears in an integral which can be evaluated analytically. Thus

$$S = -\int_0^{Z_E^*}\left[\frac{g(t)\mathscr{R}(Z^*)}{(\bar{Z}^*+Z_0^*)\,dZ^*/d\sigma} - \frac{g_0}{2\,dZ^*/d\sigma|_0}\right]\frac{dZ^*}{Z^*-Z_0^*} - \frac{g_0}{2\,dZ^*/d\sigma|_0}\int_0^{Z_E^*}\frac{dZ^*}{Z^*-Z_0^*} \tag{44}$$

where the suffix denotes quantities evaluated at $Z^* = Z_0^*$. On evaluating the second term we obtain

$$S = -\int_0^{t_E}\left[\frac{g(t)\mathscr{R}(Z^*(t))}{\bar{Z}^*(t)+Z_0^*} - \frac{g_0\,dZ^*/d\sigma}{2\,dZ^*/d\sigma|_0}\right]\frac{1}{Z^*(t)-Z_0^*}\frac{d\sigma}{dt}dt - \frac{g_0}{2\,dZ^*/d\sigma|_0}\log\left(\frac{Z_E^*-Z_0^*}{Z_0^*}\right) \tag{45}$$

Again we need to know the value of the integrand at $t=0$ before the first integral can be evaluated using Simpson's rule, this requires the limit which follows from equations (39) and (40)

$$\left.\frac{dZ^*}{d\sigma}\frac{d\sigma}{dt}\right|_{\sigma=0} = \left(\frac{7k}{3}\right)^{\frac{1}{2}}. \tag{46}$$

The value of S can now be determined for all the necessary values of Z^*. It is worth noting that the logarithm in equation (45) is interpreted in the following manner

$$\log\left(\frac{Z_E^*-Z_0^*}{Z_0^*}\right) = \log\left|\frac{Z_E^*-Z_0^*}{Z_0^*}\right| + i(\arg(Z_E^*-Z_0^*) - \arg(Z_0^*)). \tag{47}$$

The value of $\arg(Z_o^*)$ lies between 0 and $\frac{1}{2}\pi$, and the value of $\arg(Z_E^* - Z_o^*)$ increases monotonically from $\arg(Z_E^*)$ as Z_o^* moves around the sheet.

3.3. The Angular Extent of the Sheet

By using intrinsic coordinates we are unable, *a priori*, to fix the angular extent of the sheet. If the length of the trace of the sheet in the cross-flow plane is fixed then the angular extent of the trace varies considerably from solution to solution which is clearly undesirable. The parameter k introduced in equation (39) can be adjusted until a solution with the required angular extent for the trace is obtained. This is done automatically by introducing a new equation into the solution procedure which states that the angle between the line joining the vortex to the end of the trace and the y-axis must be Θ radians. Expressed in mathematical terms this gives

$$\left|\frac{Z_E - Z_V}{|Z_E - Z_V|} - e^{i\Theta}\right| = 0. \tag{48}$$

Although the value of k is not determined explicitly by equation (48), the extra equation becomes part of the set of non-linear simultaneous equations whose formulation and solution are described in the next sections.

3.4. Discretisation

The continuous unknown functions $g(t)$ and $\psi(t)$ are specified in terms of their values at a discrete set of points. The finite part of the jet-vortex sheet is divided into $2n$ equal intervals in t. The beginning of the first interval is the leading edge and the end of the last interval is the end of the finite jet-vortex sheet. The points that enclose these intervals total $2n+1$ and are called pivotal points. We also introduce $2n$ intermediate points at the centre (in t) of the $2n$ intervals just defined. The set of unknowns to be determined is formed from the $2n$ values of the sheet strength $g(t)$ measured at the intermediate points, the $2n$ values of the inclination of the tangent $\psi(t)$ also measured at the intermediate points, the three values which represent the position Z_V and strength Γ of the isolated vortex, and the constant k in equation (48). We have therefore a total of $4n+4$ unknown quantities to be determined.

We apply the pressure condition (7) and the normal velocity condition (6) at the $2n$ intermediate points. The force condition (11) and the Kutta condition (32) form three more conditions to be satisfied and the final condition comes from equation (48), which is the condition that fixes the angular extent of the sheet. We have therefore a set of $4n+4$ equations to be satisfied.

By using third order finite difference formulae it is possible to express the equations as a set of non-linear simultaneous algebraic equations in terms of the unknowns. Details of the numerical formulae used can be found in the Appendix.

3.5. Numerical Solution Procedure

The original equations which were evaluated from the boundary conditions on the sheet are recast into a set of non-linear simultaneous algebraic equations by standard techniques of numerical analysis. These equations can now be solved using the $4n+4$ dimensional form of the Newton iteration procedure. Let $\mathbf{Y}$ represent a $4n+4$ dimensional vector composed of the residuals of the equations to be satisfied, and $\mathbf{X}$ a similar vector composed of the unknowns to be calculated. To find $\mathbf{X}$ such that $\mathbf{Y}=\mathbf{0}$ we adopt the iterative procedure

$$\mathbf{X}_{k+1}=\mathbf{X}_k-A_j^{-1}\mathbf{Y}_k \tag{49}$$

where A_j is the Jacobian matrix of $\mathbf{Y}$ with respect to $\mathbf{X}$ evaluated at the jth iteration. Given a good approximation $\mathbf{X}_1$ to the solution, convergence is fast enough with $j=1$. However, convergence is monitored and a new matrix evaluated if necessary. The sequence of approximations $\mathbf{X}_k$ is assumed to have converged to a limit when

$$|\mathbf{Y}|<\varepsilon \tag{50}$$

where ε is some prescribed tolerance.

4. The Lift and the Drag

Both the lift and the drag can be considered to be the sum of two consituent parts. The first is the aerodynamic force on the wing surface which can be calculated by integrating the pressure along a control surface which just surrounds the wing. The second is the direct effect of the thrust which the jet exerts directly on the wing. In the following analysis a superscript W denotes an aerodynamic component and a superscript J denotes a thrust component. In an inviscid model no evaluation can be made of the skin friction.

4.1. Aerodynamic Forces

By representing the wing surface in the following way

$$\begin{aligned} x &= s\cot\gamma \\ y &= s\tau \\ z &= \frac{s}{2p}\left((q^4-4p^2\tau^2)^{\frac{1}{2}}-1+p^2\right) \end{aligned} \tag{51}$$

where s, τ are the independent variables, and by letting $\mathbf{R}=x\mathbf{i}+y\mathbf{j}+z\mathbf{k}$ we have the following expression for the coefficient of vector force on the wing surface, referred to the plan-form area and the free-stream kinetic pressure

$$\mathbf{C}_F^W=\frac{\tan\gamma}{s^2}\iint C_p\mathbf{R}_s X\mathbf{R}_\tau\, ds\, d\tau. \tag{52}$$

Since the axis system is inclined at an angle α to the uniform stream we obtain the following expressions for the coefficient of lift C_L^W and the coefficient of the drag C_D^W respectively

$$\begin{aligned} C_L^W &= \mathbf{C}_F^W\cdot(\mathbf{k}\cos\alpha-\mathbf{i}\sin\alpha) \\ C_D^W &= \mathbf{C}_F^W\cdot(\mathbf{i}\cos\alpha+\mathbf{k}\sin\alpha) \end{aligned} \tag{53}$$

We can now define the lift and drag parameters L^W and D^W as follows

$$L^W = \frac{C_L^W}{\tan^2\gamma} = \frac{\mathbf{C}_F^W \cdot \mathbf{k}}{\tan^2\gamma}$$

$$D^W = \frac{C_D^W}{\tan^3\gamma} = \frac{\mathbf{C}_F^W \cdot \mathbf{i}}{\tan^3\gamma} + a\frac{\mathbf{C}_F^W \cdot \mathbf{k}}{\tan^2\gamma} \tag{54}$$

since α is a small angle and the z component of $\mathbf{C}_F^W$ is an order of magnitude larger than its x component. Since the flow is conical one of the integrations in equation (52) may be performed explicitly so that we obtain

$$L^W = \int_0^{\eta_m} \frac{\Delta C_p}{\tan^2\gamma} \cos\frac{2p\eta}{q^2}\, d\eta$$

$$D^W = \frac{1}{2p}(1+2pa-p^2)L - \frac{q^2}{2p}\int_0^{\eta_m} \frac{\Delta C_p}{\tan^2\gamma}\, d\eta \tag{55}$$

where η is defined from $\tau = q^2/2p \sin(2p/q^2)\eta$ and the integration is carried out in the cross-flow plane. As the camber parameter $p \to 0$ we recover the known result for a flat plate delta wing

$$L^W = \int_0^1 \frac{\Delta C_p}{\tan^2\gamma}\, d\eta, \qquad D^W = aL^W. \tag{56}$$

4.2. The Thrust of the Jet

Let $\mathbf{T}$ be the unit vector along the initial direction of the jet. Using equations (51) we know that $\mathbf{T}$ lies in the plane of the vectors $\hat{\mathbf{R}}_s$ and $\hat{\mathbf{R}}_\tau$ for $\tau = 1$, $\hat{\mathbf{R}}_s$ and $\hat{\mathbf{R}}_\tau$ are unit vectors in the direction of the derivatives of $\mathbf{R}$ with respect to s and τ. Therefore we have,

$$\mathbf{T} = (\mu\hat{\mathbf{R}}_s + \nu\hat{\mathbf{R}}_\tau)_{\tau=1} = \mu\cos\gamma\,\mathbf{i} + \left(\mu\sin\gamma + \nu\frac{1-p^2}{q^2}\right)\mathbf{j} - \frac{2\nu p}{q^2}\mathbf{k} \tag{57}$$

where μ, ν are arbitrary constants. $\mathbf{T}$ is a unit vector lying along the initial jet direction. Expressed algebraically we have the equations $|\mathbf{T}| = 1$ and $\mathbf{T} \cdot \hat{\mathbf{R}}_s|_{\tau=1} = \cos\beta$ from which the values of μ and ν are determined.

$$\mu = \cos\beta - \frac{1-p^2}{q^2}\sin\gamma\sin\beta\left(1 + \frac{1}{2}\sin^2\gamma\frac{(1-p^2)^2}{q^4} + O(\gamma^4)\right)$$

$$\nu = \sin\beta\left(1 + \frac{1}{2}\sin^2\gamma\frac{(1-p^2)^2}{q^4} + O(\gamma^4)\right). \tag{58}$$

The reaction of the jet on the wing $\mathbf{C}_F^J = -C_\mu(\mathbf{T}\cdot\mathbf{ii} + \mathbf{T}\cdot\mathbf{kk})$. L^J and D^J are calculated from $\mathbf{C}_F^J$ in a similar manner as L^W and D^W are calculated in equations (53) and (54). By substituting the expressions for μ and ν into equations (57) and neglecting terms of $O(\gamma^2)$ compared with 1, we obtain the following expressions for L^J and D^J.

$$L^J = c\left(\frac{2p}{q^2}\sin\beta + a\gamma\cos\beta\right)$$

$$D^J = c\left(-\frac{1}{\gamma}\cos\beta + \frac{1-p^2+2pa}{q^2}\sin\beta\right). \tag{59}$$

4.3. Pressure Coefficient

The calculation of the pressure coefficient C_p follows the calculation of Barsby.[5] For the type of flow considered the pressure coefficient has been calculated by Smith[4], and is given by

$$C_p = -2\Phi_x/U - (\Phi_y^2 + \Phi_z^2)/U^2 + \alpha^2. \tag{60}$$

Since flow is conical the velocity potential satisfies the following equation

$$\Phi = x\Phi_x + y\Phi_y + z\Phi_z + \Phi_\infty \tag{61}$$

where Φ_∞ is a constant. Substituting the value of Φ_x obtained from equation (61) into equation (60) we find

$$C_p = 2(y\Phi_y + z\Phi_z - \Phi)/Ux - (\Phi_y^2 + \Phi_z^2) + \alpha^2 + 2\Phi_\infty/Ux. \tag{62}$$

The constant Φ_∞ is chosen so that the value of C_p vanishes as $y,z \to \infty$. $1/(U \tan\gamma)\Phi_y$ and $1/(U\tan\gamma)\Phi_z$ are the real and imaginary parts of dW/dZ and can be calculated from equations (37) and (38). In order to calculate Φ, equation (37) must be integrated with respect to Z^* to find an expression for the complex potential W. It can be shown that

$$\begin{aligned} W = &-i\left(\frac{q^4}{2p^2}\tan^{-1}\left(\frac{p}{\zeta + qZ^*}\right) - \frac{(1-p^2)q}{2p(q\zeta + Z^*)} + \frac{aq}{p(pZ^* - iq)}\right) \\ &-\frac{i\Gamma}{2\pi}\log\frac{Z^* - Z_V^*}{Z^* - \bar{Z}_V^*} - \frac{i}{2\pi}\int_0^{\sigma_E} g(\sigma)\log\frac{Z^* - Z^*(\sigma)}{Z^* - \bar{Z}^*(\sigma)}\,d\sigma. \end{aligned} \tag{63}$$

The value of Φ_∞ is equal to the $\lim_{Z\to\infty}(W + iaZ)Us\tan\gamma$ and is given by the following expression

$$\begin{aligned} \frac{\Phi_\infty}{Us\tan\gamma} = &-i\mathscr{R}\left(\frac{q^4}{2p^2}\tan^{-1}\frac{p^2}{i(2+p^2)} + \frac{1-p^2}{4}i + \frac{ai(2+p^2)}{2p} + \right. \\ &\left. + \frac{\Gamma}{2\pi}\log\frac{iq - pZ_V^*}{iq + p\bar{Z}_V^*} + \frac{1}{2\pi}\int_0^{\sigma_E}\log\frac{iq - pZ^*(\sigma)}{iq + p\bar{Z}^*(\sigma)}\,d\sigma\right). \end{aligned} \tag{64}$$

From expressions (63) and (64) we can determine the pressure $C_p/U\tan^2\gamma$ By substituting expressions (63) and (64) into equation (62) we can obtain a value for the pressure $C_p/U\tan^2\gamma$. The logarithms in these expressions are multi-valued and we use the device of Smith[7] to determine the appropriate value.

In the present theory no scale factors were used and the choice of ε was determined by the need to achieve accurate solutions in a reasonable amount of computing time. Rather than calculate solutions for various values of the incidence parameter a, it was felt to be more worthwhile to calculate solutions for fixed values of the lift parameter $L = L^W + L^J$. This is achieved by varying the incidence until a solution with the required lift is found. Solutions were calculated at most of the grid points determined by the following three-dimensional grid.

$$p = 0{\cdot}0(0{\cdot}1)0{\cdot}6$$
$$c = 0{\cdot}0(0{\cdot}2)1{\cdot}0$$
$$L = 1{\cdot}0(1{\cdot}0)4{\cdot}0, 6{\cdot}0, 8{\cdot}0$$

Details of all the solutions calculated are given in the Table on page 25.

There are regions in the parameter space within which it has not been possible to obtain solutions. It is well known that solutions with vortex sheets separating from the leading edge when there is no blowing cannot be obtained for values of the incidence parameter close to the incidence for which the flow is attached[9]. There are also regions in the parameter space in which the solutions found are not unique and examples of these are described in the next section. The equations solved to obtain these solutions are highly non-linear and an explanation of such behaviour as non-uniqueness or non-existence is not attempted in this report.

5. Results

5.1. Extent of the Solutions Obtained

The solutions to be calculated depend upon the following five parameters.

(i) The incidence parameter $a = \alpha/\tan\gamma$
(ii) The camber parameter p
(iii) The blowing strength $c = C_\mu/\tan^2\gamma$
(iv) The blowing angle β
(v) The wing semi-apex angle γ

The amount of work involved in the generation and analysis of solutions for variations of all five parameters is prohibitive. The aim of the present investigation is to gain some insight into the benefits of introducing a jet along the leading edges of a cambered wing. Barsby[1] showed that the maximum lift increment for a given jet strength occurs when the jet is in a direction normal to the leading edge. For the present investigation the direction of the jet was fixed to lie in a direction normal to the free stream so as to obtain the greatest lift increments without increasing the drag of the wing by directing the jet upstream. Thus the initial jet direction has the value $\beta = \frac{1}{2}\pi - O(\gamma^2)$, and substituting this value into equations (24), (30) and (59), and neglecting terms $O(\gamma^2)$ compared with unity we find that solutions now only depend on the three parameters a, p and c. The effects of varying the angular extent of the sheet and varying the number of points specifying the finite sheet shape have been investigated by Smith[7] and overall features of the flow field such as lift varied little from model to model. The values chosen for Θ and n for all solutions were held fixed at the following.

$$\Theta = 6{\cdot}0$$

$$n = 12$$

The chosen value for the tolerance ε was 10^{-6}. The choice of the tolerance must depend upon any scaling used in the formulation of the final algebraic equations.

5.2. Non Unique Solutions

In his analysis of separation from the leading edges of a cambered wing, Barsby[1] found regions in the (a, p) parameter space within which solutions could not be obtained. This region lies on either side of the line defined by $a = \frac{1}{2}p(3+p^2)$; the line for which the flow remains attached at the leading edges. For a value of $p = 0$ solutions could not be obtained for $a < 0{\cdot}2$. For values of $p > 0$ the region in which solutions could be found lay much closer to the line $a = \frac{1}{2}p(3+p^2)$ for values of $a > \frac{1}{2}p(3+p^2)$ but further away for values of $a < \frac{1}{2}p(3+p^2)$. With a more sophisticated model Barsby[2] was able to generate solutions much closer to the attachment incidence for the particular case of the flat plate. In fact a new class of solutions which separate from inboard of the leading edge were found. However in each of the cases computed the numerical model breaks down as the incidence approaches the attachment incidence.

In the present case for values of the blowing strength not equal to zero solutions could be generated for values of $a = \frac{1}{2}p(3+p^2)$. In fact solutions could be generated continuously in a region above and just below this incidence which is the attachment incidence when there is no leading edge jet. For all the solutions, the vortex system remained above the wing upper surface. The solutions in the Table with an incidence $a < \frac{1}{2}p(3+p^2)$ are marked with an asterisk.

In the case of the flat plate the attachment incidence is zero and any solution with $a > 0$ with the vortex above the wing has a similar solution with $a = -a$ with the vortex system below the wing. In Fig. 9 vortex sheets are shown for $p = 0{\cdot}0$, $a = -0{\cdot}0581$ and $0{\cdot}0519$. As the incidence decreases through zero the vortex system does not flip to the under side of the wing as expected but remains on the upper surface. There for each value of a in the range $-0{\cdot}06 < a < 0{\cdot}06$ with $p = 0$ and $c = 1{\cdot}0$ there are two solutions, one with the vortex above the wing and one with the vortex below. The differences between the two types of solution can be seen by comparing the solutions for $a = -0{\cdot}0581$ and $a = 0{\cdot}0519$ since the modulus of the incidence for these solutions is approximately the same. No experimental evidence exists to prove the existence of these solutions in a real fluid. However, Alexander[2] did comment on the tendency of the vortex system to oscillate between two states in the case of blowing from a cropped delta wing when the incidence is small. For values of $p = 0{\cdot}6$ and $c > 0{\cdot}0$, the numerical model would only converge very slowly to a solution and for higher values of p no solutions could be found at all for the values of L considered. The lack of convergence of the numerical model was associated with a numerical instability in the shape of the sheet near the leading edge. The angle of the tangent of the vortex sheet seemed to oscillate for the first few points along the sheet. This oscillation can be seen in Fig. 8 for the solution with $p = 0{\cdot}6$, $L = 4{\cdot}0$ $c = 1{\cdot}0$. The change in boundary condition which occurs as we move off the wing onto the vortex sheet implies that some form of singularity exists in the sheet shape at the leading edge. The waviness in the shape of the sheet for the higher values of the camber parameter suggests that the discrete model and distribution of points along the sheet determined by equation (39) is no longer an adequate representation for the finite vortex sheet. To achieve solutions for higher values of p it may be necessary to investigate this singularity in more detail.

5.3. Shape of the Vortex Sheet

The changes in the shape of the sheet when blowing is introduced are shown in Figs. 5, 6, 7 and 8 for values of the camber $p = 0{\cdot}0$, $0{\cdot}2$, $0{\cdot}4$ and $0{\cdot}6$ respectively. In the comparisons the lift parameter has a value of $L = 4{\cdot}0$ and the values of the blowing strength are $c = 0{\cdot}0$ and $1{\cdot}0$ for each value of p considered. The vortex systems in Fig. 5 for $p = 0{\cdot}0$ compare well with the results of Barsby[1]. The introduction of the jet expands the core region of the vortex system and moves the core centre outboard by an amount equal to about 10 per cent of the wing semi span. The sheet assumed a more circular shape and there is a marked reduction in the curvature of the sheet near the leading edge.

Similar changes in the sheet shape occur when blowing is introduced for values of $p = 0{\cdot}2$, $0{\cdot}4$, and $0{\cdot}6$ as can be seen in Figs. 6, 7 and 8. For $c = 0{\cdot}0$, as the value of p increases for constant lift, the overall size of the vortex core becomes smaller whereas for $c = 1{\cdot}0$ the relative reduction in size is much less. In the case of $p = 0{\cdot}6$, the size of the vortex core for $c = 1{\cdot}0$ is perhaps 15 times the size of the core for $c = 0{\cdot}0$. The movement outboard caused by the blowing remains about 10 per cent of the semi span for values of p up to $0{\cdot}4$ reducing to about 5 per cent for $p = 0{\cdot}6$.

The movement of the isolated vortex for varying c and p can be seen in Fig. 10 for a lift parameter of $L = 2{\cdot}0$. In general as the blowing strength increases for constant p the movement of the isolated vortex is away from the wing surface. However as p increases from zero for constant c the movement of the vortex is outboard and generally downward. Variations of the vortex position with c and p for the other values of the lift parameter L in the Table do not differ significantly from the pattern shown in Fig. 10.

5.4. Pressure Distributions

In Figs. 11, 12 and 13 the pressure distributions across part of the wing surface can be seen for a value of the lift parameter $L = 4{\cdot}0$. In Fig. 11 we see that for a flat plate wing the suction peak is more outboard and increased by the introduction of blowing. In Figs. 12 and 13 for values of the camber parameter $p = 0{\cdot}2$ and $0{\cdot}4$ respectively although the peak is still moved outboard, there is no longer an increase in the height of the peak. In all three cases the overall width of the peak is not dramatically changed by the introduction of blowing.

The pressure jump across the wing surface at the leading edge is zero in the no-blowing cases. For values of c not equal to zero the pressure jump is proportional to c and is given by equation (18). The introduction of blowing thus reduces the adverse pressure gradient at the leading edge and reduces the likelihood of a secondary separation. Alexander[11] used this mechanism to remove secondary separation.

Although leading-edge blowing increases the size of the suction peak, it also shifts the peak outboard so that not all the peak remains directly over the wing surface. This phenomenon reduces the effectiveness of blowing. On the other hand wings with camber have, for some positive values of the incidence, a component of the surface normal which points upstream. This effect is greatest at the leading edge and any suction peak over this part of the wing surface must significantly reduce the drag. The movement of the suction outboard over the leading edge has a beneficial effect on the drag; an effect which becomes more marked as the camber is increased. In some of the cases considered the calculated drag is negative.

5.5. Benefits of Camber and Downward Jet Deflection

An assessment of whether leading-edge blowing is beneficial in any particular context is beyond the scope of the present treatment, since it may involve considerations of engine design, ducting weight, jet noise and operational flexibility. What can be assessed within the present treatment is whether the combination of camber of the wing cross-section and downward inclination of the jet from the leading edge makes leading-edge blowing more attractive. Three different situations are considered below.

The situation in which leading-edge blowing is most obviously worthy of consideration arises when the engine thrust is determined by the need to overcome the drag at the cruising condition, so that air can be made available from the engines in the take-off and landing phases in order to augment the lift. The quantity of interest is the increment in lift coefficient that can be produced by a certain coefficient of blowing momentum on a wing at a given angle of incidence, since the possibilities of increasing the lift coefficient by increasing the angle of incidence have already been explored. In the present notation, the quantity to be examined is ΔL, where $\Delta L = L(a, p, c) - L(a, p, 0)$, L being regarded as a function of the incidence, camber and blowing parameters, a, p and c. Values of ΔL can be found for each combination of p and c by plotting the tabulated values of L against a. ΔL is obviously a function of p and c; it is more meaningful to regard its variation for fixed p and c as depending on $L_0 = L(a, p, 0)$ than on a itself.

It is found that ΔL does not vary much with L_0. Figs 14 and 15 show the band within which the values of ΔL lie for the range of values of L_0 covered by the calculations. For the more highly cambered wing ($p = 0{\cdot}6$), the band is extremely narrow and the lift increment is closely proportional to the blowing momentum. For the less cambered wing ($p = 0{\cdot}2$), the band is somewhat wider. The initial increase of lift with blowing is more rapid than for the more cambered wing, but this rate of increase is not maintained at the higher blowing momenta. Since the variation of ΔL with L_0 is small, the effect of camber on ΔL can be seen from a plot for a single value of L_0. Fig. 16 is drawn for $L_0 = 5$ (corresponding to $C_L = 0{\cdot}5$ on a wing of aspect ratio $1{\cdot}26$). It shows that the combination of camber and downward jet deflection has little effect on the lift increment produced by a given blowing momentum. Hence we can write approximately

$$\Delta L \doteqdot \Delta L(c)$$

and so

$$L(a,p,c) \doteqdot L(a,p,0) + L(a,0,c) - L(a,0,0),$$

i.e. the effects of camber and of blowing on lift are approximately additive. For this first situation therefore, the combination of wing camber and downward jet deflection produces no advantage over the plane wing.

If, on the other hand, there is no engine thrust to spare at take-off, leading-edge blowing is inherently less attractive. However, it is still of interest to examine whether the combination of camber and jet deflection offers any advantage. In this situation it is clear that the change in drag is as significant as the change in lift. In Fig. 17 the drag parameter $D(= C_D/\tan^3 \gamma)$ is shown for the wings of Fig. 16, i.e. for four wings of different amounts of camber, each set at an angle of incidence which produces $L = 5$ in the absence of blowing. The drags are, of course, different even in the absence of blowing, being smaller for the more highly cambered wings. As the blowing momentum increases these differences increase markedly and the advantage of camber becomes more pronounced. Fig. 18 combines the information from Figs. 16 and 17. It still relates to the same four wings at their particular angles of incidence, but the drag is now shown as a function of the lift, with the required blowing momenta shown by an intersecting family of curves. It is clear that, when drag is significant, the combination of camber and jet deflection does make leading-edge blowing more attractive as a means of increasing lift at fixed incidence. Fig. 18 also suggests that values of the camber parameter p larger than $0{\cdot}6$ may be of interest, at least for the larger rates of blowing.

A third possible situation is that, with blowing nozzles installed for reasons of airfield performance, leading-edge blowing might be used away from the ground, when the angle of incidence is no longer limited. Interest then centres on the drag which has to be overcome in order to produce the required lift, at a given level of blowing momentum. Figs. 19–21 show the variation of the drag parameter D with the degree of camber for values of the lift parameter, L, of 1, 2 and 4, (for $c = 0$, the present solutions have been supplemented by results from ref. 5). Without blowing, the variation is as described in ref. 5: for the smaller values of L the drag falls as the camber parameter increases from zero, reaches a minimum and then rises slightly again; while for $L = 4$ the drag falls steadily as the degree of camber increases. With blowing which is not too large in relation to the level of the lift, the drag falls steadily as the camber increases, the plots for larger values of L resembling Fig. 19. For large blowing rates at small values of the lift, the drag falls to a minimum and then rises again quite sharply. This combination of low lift and strong blow is unlikely to be of any practical interest. The more typical behaviour is that the reduction in drag at fixed lift produced by a certain blowing momentum increases as the degree of camber increases. For example, for $L = 4$, the drag of the uncambered, unblown wing is reduced by about a third either by blowing with $c = 0{\cdot}8$ or by cambering with $p = 0{\cdot}6$, while the combination of the same amounts of blow and camber reduces the drag to zero. Thus we see that the combination of wing camber and downward jet deflection adds very significantly to the attractiveness of leading-edge blowing in this context.

To help in assessing the benefits of blowing in this situation where the angle of incidence is not of direct importance, an attempt has been made to summarize the dependence of the drag parameter on the parameters defining the lift, camber and blowing. By ignoring the values for low lift and strong blow a simple expression can be fitted fairly closely to the numerical results;

$$D \doteqdot 0{\cdot}011^2(11-0{\cdot}025L^2)-0{\cdot}16Lc-p(0{\cdot}3(L-0{\cdot}5)+0{\cdot}2Lc) \tag{65}$$

for $0 \leq c \leq 1$, $1 \leq L \leq 8$ and $p \leq \max(0{\cdot}6; (0{\cdot}7-0{\cdot}5c)L)$. To test the validity of the expression, the values of D from the tabulated solutions have been plotted as D_{exact} against the values of D from equation (65) as D_{approx} in Fig. 22 for $p=0$, $0{\cdot}2$, $0{\cdot}4$, $0{\cdot}6$, $c=0$, $0{\cdot}4$, $0{\cdot}8$, and $L=1$, 2, 4, 6, 8. The absolute error is small throughout, but the relative error can be large near $D=0$.

It must be remembered that the present results have all been obtained for blowing in a direction which is essentially normal to the free stream, since this was found previously[5] to give the largest lift increments. If drag is of importance, then it may be that a more effective compromise might be achieved with the blowing momentum directed rearward as well as downward. The present results shed no light on this and so the assessment of the contribution of camber and downward jet deflection remains incomplete in this respect.

The present results are for configurations in which the downward deflection of the jet is fixed by the camber of the wing. Since the advantages shown for these configurations relative to the plane wing relate to reduced drag at fixed lift rather than to increased lift at fixed incidence, it may be conjectured that the camber is playing a bigger role than the downward deflection of the jet. For a wing with thickness, the downward deflection of the jet may be varied, so calculations for such a configuration might be rewarding.

6. Conclusions

Previous studies of leading-edge blowing from a flat-plate delta wing and of leading-edge separation from a wing with conical camber have been extended to treat leading-edge blowing from a delta wing with conical camber. Solutions have been obtained for wide ranges of values of blowing momentum, lift and camber, for a jet which emerges tangentially to the wing surface and normal to the free stream. The strength and position of the vortex and the incidence, lift and drag of the wing have been tabulated for the solutions found.

Contrary to expectation, the downward deflection of the jet which is associated with the camber does not produce a lift increment due to blowing which is significantly larger than the increment produced by the same blowing momentum on a plane wing. On the other hand, the drag increment which goes with this lift increment is much smaller for the cambered wing and is negative for large camber. Any assessment of the application of leading-edge blowing in a situation in which thrust is limited should therefore include the benefits which arise from the combination of wing camber and downward jet deflection.

The use of the present model of the flow for a thin wing does not enable the effects of camber and downward deflection to be distinguished. This is a suitable topic for further work, which should also cover the effects of rearward deflection of the jet momentum for cambered wings.

Acknowledgements

This work was initially financed by a Science Research Council research grant at the University of East Anglia, and was completed at Liverpool University. The author wishes to thank Professor N. Riley of U.E.A. and J. H. B. Smith of R.E.A. Farnborough for their guidance and help.

LIST OF SYMBOLS

a	Incidence parameter, $a = \alpha/\tan\gamma$
c	Blowing strength parameter, $c = C_\mu/\tan^2\gamma$
C_p	Pressure coefficient
C_L	Lift coefficient
C_D	Drag coefficient
C_μ	Blowing coefficient
D	Drag, $D = C_D/\tan^3\gamma$
f	Dimensional force per unit length in the x-direction sustained by the isolated vortex and cut
F	Non-dimensional form of f, $F = f/\frac{1}{2}\rho U^2 s \tan^2\gamma$
g	Sheet strength, $g(t) = -\dfrac{1}{Us\tan\gamma}\dfrac{d\Delta\Phi}{d\sigma}$
G	Pressure jump across sheet, $G = -\Delta C_p/\tan^2\gamma$
I, I_R	Integrals used to calculate the force F
I_1, I_2	Integrals, $I_1 = \int \cos\psi \, d\sigma$, $I_2 = \int \sin\psi \, d\sigma$
k	Parameter used to fix the angular extent of the sheet in equations (39). k is determined by numerical procedure
L	Lift, $L = C_L/\tan^2\gamma$
M	Blowing constant
$\mathbf{n}$	Normal to trace of sheet in cross-flow plane
n	Integer to determine the number of intervals along the finite jet-vortex sheet parameter
p	Camber parameter
P	Pressure, $P = C_p/\tan^2\gamma$
q	Parameter, $q = \sqrt{(1+p^2)}$
r	Polar coordinate
$\mathbf{R}$	Shape of wing surface
s	Semi span of wing projection
$\mathbf{S}$	Shape of stream surface
t	Independent parameter along trace of sheet
$\tilde{t}$	Independent parameter along geodesic
$\mathbf{T}$	Tangent vector to three-dimensional sheet surface
U	Free stream speed
u, v	Coordinates used in unrolled sheet surface
$\mathbf{V}$	Velocity of fluid
V_j	Speed of jet fluid
W	Complex potential
x, y, z	Cartesian coordinates
X_j, Y_j	The set of variables to be calculated and equations to be solved
Z	Complex representation of cross-flow plane, $Z = (y + iz)/s$

Z^*	Complex coordinate, $Z^* = \surd(\zeta^2 - 1)$
α	Incidence
β	Blowing angle
γ	Semi-apex angle of projection of wing
Γ	Strength of isolated vortex
δ_J	Width of jet
Δ	Difference operator across the sheet (inside–outside)
ε	Tolerance used in iteration procedure
ζ	Complex coordinate, $\zeta = (Z - ip)/(1 - ipZ)$
θ	Polar coordinate
Θ	Parameters used to fix the angular extent of the sheet, for all solutions in this paper Θ was set to 6·0
κ	Curvature of geodesic
ρ	Density of fluid
ρ_J	Density of jet fluid
σ	Arc length of trace of sheet in cross-flow plane
σ^*	Arc length of trace in Z^*-plane
τ	Independent parameter along trace of wing surface in cross-flow plane
ξ, χ	Parameters used in the calculation of F
ϕ	Angle between radius vector and tangent
Φ	Disturbance potential
Φ_{σ_m}	Mean of tangential velocities on either side of the sheet
ψ	Angle of tangent
Ψ	Stream function
μ, ν	Parameters used to calculate L^J and D^J

REFERENCES

No.	Author(s)	Title, etc.
1	J. E. Barsby	Calculations of the effect of blowing from the leading edges of a slender delta wing. A.R.C. R. & M. No. 3692 (1972)
2	A. J. Alexander	Experimental investigation on a cropped delta wing with leading-edge blowing. COA Report Vol. 162, Cranfield (1963)
3	W. J. G. Trebble	Exploratory investigation of the effects of blowing from the leading edge of a delta wing. A.R.C. R. & M. No. 3518 (1966)
4	J. H. B. Smith	The properties of a thin conically cambered wing according to slender body theory. A.R.C. R. & M. No. 3135 (1960)
5	J. E. Barsby	Flow past conically-cambered slender delta wings with leading-edge separation. A.R.C. R. & M. No. 3748 (1974)
6	L. C. Squire	Camber effects on the non-linear lift of slender wings with sharp leading edges. A.R.C. C.P. No. 924 (1966)
7	J. H. B. Smith	Improved calculations of leading-edge separation from slender delta wings. *Proc. Roy. Soc. A.*, Vol. 306, 67–90 (1968)
8	D. A. Spence	The lift coefficient of a thin, jet-flapped wing. *Proc. Roy. Soc.*, Vol. 238, 46–68 (1956)
9	J. E. Barsby	Separated flow past a slender delta wing at low incidence. *The Aeronautical Quarterly*, Vol. 24 (May 1973)
10	E. C. Maskell	Discussion at the symposium on vortex motions organised by IUTAM in 1964. *Progress in Aeronautical Sciences* Vol. 7, 44, Pergamon (1966)
11	A. J. Alexander	Experiments on a delta wing using leading-edge blowing to remove the secondary separation. COA Report Vol. 161, Cranfield (1963)

APPENDIX

Details of Numerical Procedure

The following analysis is intended to layout briefly the numerical techniques adopted to transform the conditions to be satisfied into a set of $4n+4$ simultaneous non-linear equations in the $4n+4$ unknowns. The value of ψ at the jth pivotal point is denoted by ψ_j, and the value of ψ at the jth intermediate point is denoted by $\tilde{\psi}_j$. The value of ψ at the leading edge is denoted by ψ_0.

The sheet is divided into intervals determined by the following values of the independent variable t.

$$t_j = hj \qquad j = 0, 1, \ldots, 2n$$
$$\tilde{t}_j = h(j-\tfrac{1}{2}) \qquad j = 1, 2, \ldots, 2n$$

In the present case the value chosen for n was 12 and the value for h was 0·1. The following $4n+4$ quantities are the unknowns to be calculated from the procedure described in Section 3·5

$$\tilde{\psi}_j \qquad j = 1, 2, \ldots, 2n$$
$$\tilde{g}_j \qquad j = 1, 2, \ldots, 2n$$
$$Z_V, \Gamma, \ \kappa$$

The values of σ at the pivotal and intermediate points can be calculated from equation (39). We now define two derivatives $D(t) = d\delta/dt$ and $K(t) = d\psi/dt$. The values of ψ and D at the pivotal points and K and D at the intermediate points are calculated as follows.

$$\psi_0 = \sin^{-1}(-2p/q^2)$$
$$\psi_1 = (-4\psi_0 + 15\tilde{\psi}_1 + 10\tilde{\psi}_2 - \tilde{\psi}_3)/20$$
$$\psi_j = (-\tilde{\psi}_{j-1} + 9\tilde{\psi}_j + 9\tilde{\psi}_{j+1} - \tilde{\psi}_{j+2})/16 \qquad j = 2, 3, \ldots, 2n-2$$
$$\psi_{2n-1} = (+\tilde{\psi}_{2n-3} - 5\tilde{\psi}_{2n-2} + 15\tilde{\psi}_{2n-1} + 5\tilde{\psi}_{2n})/16$$
$$\psi_{2n} = (-5\tilde{\psi}_{2n-3} + 21\tilde{\psi}_{2n-2} - 35\tilde{\psi}_{2n-1} + 35\tilde{\psi}_{2n})/16$$
$$D_j = \frac{kt_j(14-10t_j+t_j^2)}{6(1+t_j)^2} \qquad j = 0, 1, \ldots, 2n$$
$$\tilde{D}_j = \frac{k\tilde{t}_j(14-10\tilde{t}_j+\tilde{t}_j^2)}{6(1+\tilde{t}_j)^2} \qquad j = 1, 2, \ldots, 2n$$
$$\tilde{K} = (-32\psi_0 + 15\tilde{\psi}_1 + 20\tilde{\psi}_2 - 3\tilde{\psi}_3)/(30h)$$
$$\tilde{K}_2 = (16\psi_0 - 45\tilde{\psi}_1 + 20\tilde{\psi}_2 + 9\tilde{\psi}_3)/(30h)$$
$$\tilde{K}_j = (\tilde{\psi}_{j-2} - 8\tilde{\psi}_{j-1} + 8\tilde{\psi}_{j+1} - \tilde{\psi}_{j+2})/(12h) \qquad j = 3, 4, \ldots, 2n-2$$
$$\tilde{K}_{2n-1} = (\tilde{\psi}_{2n-3} - 6\tilde{\psi}_{2n-2} + 3\tilde{\psi}_{2n-1} + 2\tilde{\psi}_{2n})/(6h)$$
$$\tilde{K}_{2n} = (-\tilde{\psi}_{2n-3} + 9\tilde{\psi}_{2n+2} - 18\tilde{\psi}_{2n-1} + 11\tilde{\psi}_{2n})/(6h)$$

The coordinates of the intermediate and pivotal points in the cross-flow plane can now be calculated.

$$Z_0 = 1{\cdot}0$$
$$Z_j = Z_{j-1} + (D_{j-1}\,e^{i\psi_{j-1}} + 4\tilde{D}_j\,e^{i\tilde{\psi}_j} + D_j\,e^{i\psi_j})h/6 \qquad j = 1, 2, \ldots, 2n$$
$$\tilde{Z}_1 = Z_0 + (9D_0\,e^{i\psi_0} + 19\tilde{D}_1\,e^{i\tilde{\psi}_1} - 5D_1\,e^{i\psi_1} + \tilde{D}_2\,e^{i\tilde{\psi}_2})h/48$$
$$\tilde{Z}_j = \tilde{Z}_{j-1} + (\tilde{D}_{j-1}\,e^{i\tilde{\psi}_{j-1}} + 4D_{j-1}\,e^{i\psi_{j-1}} + \tilde{D}_j\,e^{i\tilde{\psi}_j})h/6 \qquad j = 2, 3, \ldots, 2n$$

The coordinates of the pivotal and intermediate points in the ζ plane and in the Z^* plane can be calculated using equations (34) and (35).

The value of the sheet strength at the pivotal points and at the leading edge are as follows.

$$g_0=(35\tilde{g}_1-35\tilde{g}_2+21\tilde{g}_3-5\tilde{g}_4)/16$$
$$g_1=(-4g_0+15\tilde{g}_1+10\tilde{g}_2-\tilde{g}_3)/20$$
$$g_j=(-\tilde{g}_{j-3}+9\tilde{g}_{j-2}+9\tilde{g}_{j-1}-\tilde{g}_j)/16 \qquad j=2,3,\dots,2n-2$$
$$g_{2n-1}=(\tilde{g}_{2n-3}-5\tilde{g}_{2n-2}+15\tilde{g}_{2n-1}+5\tilde{g}_{2n})/16$$
$$g_{2n}=(-5\tilde{g}_{2n-3}+21\tilde{g}_{2n-2}-35\tilde{g}_{2n-1}+35\tilde{g}_{2n})/16$$

If we define $M(t)=-\Delta\Phi/(Us\tan\gamma)$, then we can determine the values of $M(t)$ at the intermediate points.

$$\tilde{M}_{2n}=\Gamma+(9g_{2n}+19\tilde{g}_{2n}-5g_{2n-1}+\tilde{g}_{2n-1})h/48$$
$$\tilde{M}_{2n-j}=\tilde{M}_{2n-j+1}+(\tilde{g}_{2n-j}+4g_{2n-j}+\tilde{g}_{2n-j-1})h/6 \qquad j=1,2,\dots,2n-1$$

We can represent the terms in equation (37) for the complex velocity dW/dZ^* by the sum of three functions A, B and E_j. The function A is composed of the first two terms in equation (37), the function B is the isolated vortex term and the function E_j, $j=1, 2, 3$ is the Cauchy Principal Value integral and is evaluated in three different ways as described in Sect. 3.3.

$$A(Z_a,Z_b)=-\frac{pq((3+p^2)Z_a+2qZ_b)}{2Z_a(qZ_a+Z_b)^2}-\frac{iaq}{(pZ_b-iq)^2}$$
$$B(Z_a)=\frac{2\Gamma\mathcal{R}(Z_V^*)}{(Z_a-Z_V^*)(Z_a+\bar{Z}_V^*)}$$
$$E_1(Z_a)=\frac{h}{3}\sum_{j=0}^{2n}\frac{\varepsilon_jD_jg_j\mathcal{R}(Z_j^*)}{(Z_a-Z_j^*)(Z_a-\bar{Z}_j^*)}$$
$$E_2(Z_a)=\frac{h}{3}\left(-2g_0\left(\frac{k}{3}\right)^{\frac{1}{2}}+\sum_{j=1}^{2n}\frac{\varepsilon_jD_jg_j\mathcal{R}(Z_j^*)}{(Z_a-Z_j^*)(Z_a-\bar{Z}_j^*)}\right)$$
$$E_3(Z_a,Z_b,Z_c)=\frac{h}{3}\left(Z_bZ_c+\sum_{j=1}^{2n}\left(\frac{2g_j\mathcal{R}(Z_j^*)}{(Z_a+\bar{Z}_j^*)}-Z_bH_j\right)\varepsilon_jD_j/(Z_a-Z_j^*)\right)$$
$$-Z_b\left(\log\left|\frac{Z_{2n}^*-Z_a}{Z_a}\right|+i\left(\arg(Z_{2n}^*-Z_a)-\arg Z_a\right)\right)$$

where

$$H(t)=\frac{dZ^*}{d\sigma}=\frac{dZ^*}{d\zeta}\frac{d\zeta}{dZ}\frac{dZ}{d\sigma}=\frac{dZ^*}{d\zeta}\frac{d\zeta}{dZ}e^{i\psi}$$
$$\varepsilon_0=1$$
$$\varepsilon_{2j-1}=4 \qquad j=1,2,\dots,n$$
$$\varepsilon_{2j}=2 \qquad j=1,2,\dots,n-1$$
$$\varepsilon_{2n}=1$$

Care must be taken in evaluating $\arg(Z_{2n}-Z_a)$ since this function increases monotonically as Z_a moves along the sheet from the leading edge.

We have now defined all the quantities used in the conditions to be satisfied, and these conditions can be expressed as follows.

The pressure condition (7)

$$0=-\tilde{D}_j\tilde{g}_j\mathcal{R}\left(e^{i\tilde{\psi}_j}\tilde{Z}_j-\tilde{H}_j\left(-iA(\tilde{\zeta}_j,\tilde{Z}_j^*)+\frac{1}{2\pi i}\left(B(\tilde{Z}_j^*)+E_3\left(\tilde{Z}_j^*,\frac{\tilde{g}_j}{\tilde{H}_j},\sqrt{\frac{7k}{3}}\right)\right)\right)\right)-\tilde{M}_j\tilde{D}_j+\tfrac{1}{2}c\tilde{K}_j \qquad j=1,2,\dots,2$$

The normal velocity condition (6)

$$0 = \mathscr{I}\left(e^{i\tilde{\psi}_j}\tilde{\bar{Z}}_j - \tilde{H}_j\left(-iA(\tilde{\zeta}_j, \tilde{Z}_j^*) + \frac{1}{2\pi i}\left(B(\tilde{Z}_j^*) + E_3\left(\tilde{Z}_j^*, \frac{\tilde{g}_j}{\tilde{H}_j}, \sqrt{\frac{7k}{3}}\right)\right)\right)\right) \qquad j = 1, 2, \ldots, n$$

The force condition (11), a complex equation which gives two real conditions

$$\begin{aligned} 0 = {} & (2\bar{Z}_V - \bar{Z}_E - \bar{i}c\, e^{\bar{i}\psi_{2n}}/(2\Gamma))Z_V^* q^2/(\zeta_V(1+ip\zeta_V)^2) \\ & + iA(\zeta_V, Z_V^*) - \frac{1}{2\pi i}E_1(Z_V^*) - \frac{\Gamma}{4\pi i}\left(\frac{2ip\zeta_V^3 - 3ip\zeta_V - 1}{(1+ip\zeta_V)\zeta_V^2 Z_V^*} - \frac{1}{(Z_V^*)}\right) \end{aligned}$$

The Kutta condition (32)

$$0 = \left(-iA(\zeta_0, Z_0^*) + \frac{1}{2\pi i}B(Z_0^*) + E_2(Z_0^*)\right)$$

The condition which fixes the angular extent of the sheet (48)

$$0 = \left|\frac{Z_{2n} - Z_V}{|Z_{2n} - Z_V|} - e^{i\Theta}\right|$$

TABLE

Camber p	Blowing strength c	L	Incidence a	Drag D	Total circulation TC	Position and strength of vortex y/s	z/s	Γ
0·00	0·00	1·00	0·1335	0·1335	0·4977	0·9357	0·0316	0·4110
0·00	0·00	2·00	0·2464	0·4927	0·9686	0·8964	0·0589	0·7420
0·00	0·00	3·00	0·3480	1·0444	1·4167	0·8662	0·0841	1·0288
0·00	0·00	4·00	0·4416	1·7662	1·8468	0·8414	0·1076	1·2867
0·00	0·00	6·00	0·6120	3·6722	2·6724	0·8023	0·1512	1·7521
0·00	0·00	8·00	0·7667	6·1340	3·4670	0·7731	0·1906	2·1812
0·00	0·20	1·00	0·0713	0·0713	0·6989	0·9736	0·0681	1·0071
0·00	0·20	2·00	0·1859	0·3719	1·0415	0·9539	0·0783	1·1846
0·00	0·20	3·00	0·2900	0·8701	1·4288	0·9295	0·0932	1·3955
0·00	0·20	4·00	0·3859	1·5435	1·8361	0·9029	0·1109	1·6152
0·00	0·20	6·00	0·5609	3·3651	2·6502	0·8545	0·1491	2·0405
0·00	0·20	8·00	0·7191	5·7530	3·4421	0·8162	0·1863	2·4417
0·00	0·40	1·00	0·0256	0·0256	0·8445	0·9738	0·0983	1·4423
0·00	0·40	2·00	0·1473	0·2947	1·1383	0·9612	0·0980	1·5541
0·00	0·40	3·00	0·2523	0·7571	1·4862	0·9436	0·1076	1·7194
0·00	0·40	4·00	0·3485	1·3941	1·8591	0·9239	0·1206	1·9057
0·00	0·40	6·00	0·5238	3·1430	2·6387	0·8821	0·1522	2·2952
0·00	0·40	8·00	0·6833	5·4667	3·4200	0·8435	0·1860	2·6774
0·00	0·60	1·00	−0·0115	−0·0115	0·9442	0·9774	0·1249	1·8105*
0·00	0·60	2·00	0·1122	0·2243	1·2230	0·9645	0·1171	1·8847
0·00	0·60	3·00	0·2200	0·6602	1·5455	0·9508	0·1216	2·0184
0·00	0·60	4·00	0·3171	1·2685	1·8963	0·9345	0·1313	2·1790
0·00	0·60	6·00	0·4930	2·9581	2·6416	0·8990	0·1576	2·5348
0·00	0·60	8·00	0·6525	5·2203	3·4058	0·8633	0·1879	2·8986
0·00	0·80	1·00	−0·0388	−0·0388	1·0127	0·9859	0·1480	2·1386*
0·00	0·80	2·00	0·0801	0·1602	1·2941	0·9678	0·1355	2·1893
0·00	0·80	3·00	0·1901	0·5704	1·6014	0·9555	0·1356	2·2980
0·00	0·80	4·00	0·2888	1·1552	1·9364	0·9416	0·1422	2·4391
0·00	0·80	6·00	0·4658	2·7947	2·6539	0·9104	0·1641	2·7646
0·00	0·80	8·00	0·6255	5·0037	3·3998	0·8779	0·1911	3·1106
0·00	1·00	1·00	−0·0581	−0·0581	1·0956	0·9979	0·1670	2·4409*
0·00	1·00	2·00	0·0519	0·1036	1·3533	0·9722	0·1530	2·4746
0·00	1·00	3·00	0·1622	0·4865	1·6530	0·9593	0·1493	2·5633
0·00	1·00	4·00	0·2624	1·0498	1·9763	0·9469	0·1531	2·6876
0·00	1·00	6·00	0·4407	2·6444	2·6712	0·9188	0·1711	2·9870
0·00	1·00	8·00	0·6009	4·8070	3·3999	0·8891	0·1952	3·3156

* Asterisk denotes vortex on 'wrong' side.

TABLE—(contd.)

Camber p	Blowing strength c	L	Incidence a	Drag D	Total circulation TC	Position and strength of vortex y/s	z/s	Γ
0·10	0·00	1·00	0·2644	0·1127	0·4029	0·9546	0·0337	0·3424
0·10	0·00	2·00	0·3779	0·4491	0·8809	0·9197	0·0663	0·6932
0·10	0·00	3·00	0·4784	0·9776	1·3376	0·8926	0·0949	0·9978
0·10	0·00	4·00	0·5700	1·6753	1·7763	0·8698	0·1212	1·2708
0·10	0·00	6·00	0·7351	3·5214	2·6132	0·8323	0·1690	1·5739
0·10	0·00	8·00	0·8834	5·9043	3·4112	0·8027	0·2119	2·1864
0·10	0·20	1·00	0·1922	0·0246	0·6507	0·9847	0·0711	0·9925
0·10	0·20	2·00	0·3178	0·3080	0·9493	0·9750	0·0764	1·1486
0·10	0·20	3·00	0·4215	0·7771	1·3278	0·9578	0·0929	1·3668
0·10	0·20	4·00	0·5151	1·4182	1·7359	0·9354	0·1133	1·5941
0·10	0·20	6·00	0·6841	3·1663	2·5595	0·8910	0·1567	2·0376
0·10	0·20	8·00	0·8353	5·4612	3·3591	0·8534	0·1988	2·4487
0·10	0·40	1·00	0·1562	−0·0113	0·7860	1·0020	0·1017	1·4478
0·10	0·40	2·00	0·2715	0·2078	1·0639	0·9813	0·0988	1·5329
0·10	0·40	3·00	0·3812	0·6439	1·3883	0·9701	0·1061	1·6958
0·10	0·40	4·00	0·4770	1·2468	1·7534	0·9559	0·1199	1·8892
0·10	0·40	6·00	0·6466	2·9087	2·5310	0·9204	0·1552	2·2900
0·10	0·40	8·00	0·7989	5·1263	3·3154	0·8842	0·1932	2·6806
0·10	0·60	1·00	0·1233	−0·0413	0·8617	1·0169	0·1254	1·8266*
0·10	0·60	2·00	0·2348	0·1325	1·1503	0·9904	0·1194	1·8758
0·10	0·60	3·00	0·3441	0·5254	1·4525	0·9772	0·1211	1·9986
0·10	0·60	4·00	0·4431	1·0990	1·7896	0·9859	0·1299	2·1634
0·10	0·60	6·00	0·6149	2·6948	2·5242	0·9379	0·1581	2·5301
0·10	0·60	8·00	0·7674	4·8396	3·2858	0·9060	0·1917	2·9002
0·10	0·80	1·00	0·0914	−0·0678	0·9147	1·0305	0·1464	2·1656*
0·10	0·80	2·00	0·2064	0·0772	1·2108	1·0021	0·1368	2·1905
0·10	0·80	3·00	0·3112	0·4234	1·5092	0·9845	0·1360	2·2844
0·10	0·80	4·00	0·4112	0·9634	1·8291	0·9731	0·1410	2·4236
0·10	0·80	6·00	0·5863	2·5046	2·5297	0·9494	0·1632	2·7596
0·10	0·80	8·00	0·7394	4·5867	3·2677	0·9217	0·1927	3·1112
0·10	1·00	1·00	0·0622	−0·0893	0·9519	1·0438	0·1653	2·4765*
0·10	1·00	2·00	0·1796	0·0272	1·2557	1·0135	0·1527	2·4851
0·10	1·00	3·00	0·2826	0·3373	1·5561	0·9930	0·1499	2·5567
0·10	1·00	4·00	0·3816	0·8402	1·8668	0·9798	0·1524	2·6740
0·10	1·00	6·00	0·5593	2·3283	2·5417	0·9580	0·1695	2·9806
0·10	1·00	8·00	0·7138	4·3576	3·2588	0·9335	0·1953	3·3155

* Asterisk denotes vortex on 'wrong' side.

TABLE—(contd.)

Camber p	Blowing strength c	L	Incidence a	Drag D	Total circulation TC	Position and strength of vortex y/s	z/s	Γ
0·20	0·00	1·00	0·3953	0·0969	0·2956	0·9725	0·0296	0·2602
0·20	0·00	2·00	0·5112	0·4068	0·7709	0·9442	0·0658	0·6289
0·20	0·00	3·00	0·6121	0·9086	1·2327	0·9220	0·0967	0·9550
0·20	0·00	4·00	0·7030	1·5798	1·6796	0·9026	0·1249	1·2487
0·20	0·00	6·00	0·8645	3·3683	2·5330	0·8690	0·1761	1·7646
0·20	0·00	8·00	1·0075	5·6805	3·3422	0·8401	0·2226	2·2144
0·20	0·20	1·00	0·3266	0·0011	0·6248	1·0115	0·0733	1·0397
0·20	0·20	2·00	0·4519	0·2492	0·8724	0·9947	0·0718	1·1214
0·20	0·20	3·00	0·5565	0·6862	1·2229	0·9805	0·0869	1·3282
0·20	0·20	4·00	0·6504	1·2962	1·6183	0·9658	0·1067	1·5663
0·20	0·20	6·00	0·8159	2·9737	2·4471	0·9297	0·1529	2·0361
0·20	0·20	8·00	0·9615	5·1885	3·2593	0·8957	0·1988	2·4711
0·20	0·40	1·00	0·2798	−0·0491	0·7453	1·0273	0·1004	1·4885*
0·20	0·40	2·00	0·4080	0·1495	0·9991	1·0084	0·0938	1·5386
0·20	0·40	3·00	0·5151	0·5402	1·3019	0·9948	0·0999	1·6764
0·20	0·40	4·00	0·6110	1·1055	1·6483	0·9828	0·1129	1·8659
0·20	0·40	6·00	0·7790	2·6911	2·4091	0·9575	0·1475	2·2877
0·20	0·40	8·00	0·9260	4·8169	3·1967	0·9273	0·1880	2·6984
0·20	0·60	1·00	0·2401	−0·0824	0·8119	1·0421	0·1210	1·8584*
0·20	0·60	2·00	0·3676	0·0662	1·0847	1·0206	0·1134	1·8976
0·20	0·60	3·00	0·4788	0·4205	1·3725	1·0064	0·1140	1·9974
0·20	0·60	4·00	0·5757	0·9439	1·6936	0·9944	0·1224	2·1503
0·20	0·60	6·00	0·7467	2·4557	2·4035	0·9728	0·1493	2·5262
0·20	0·60	8·00	0·8949	4·5010	3·1568	0·9485	0·1835	2·9159
0·20	0·80	1·00	0·2065	−0·1025	0·8495	1·0579	0·1383	2·1853*
0·20	0·80	2·00	0·3312	−0·0022	1·1418	1·0330	0·1302	2·2198
0·20	0·80	3·00	0·4441	0·3127	1·4293	1·0168	0·1280	2·2962
0·20	0·80	4·00	0·5435	0·8027	1·7368	1·0046	0·1326	2·4218
0·20	0·80	6·00	0·7165	2·2431	2·4117	0·9837	0·1539	2·7553
0·20	0·80	8·00	0·8667	4·2230	3·1346	0·9630	0·1830	3·1243
0·20	1·00	1·00	0·1780	−0·1124	0·8661	1·0757	0·1529	2·4817*
0·20	1·00	2·00	0·2978	−0·0586	1·1798	1·0455	0·1451	2·5164*
0·20	1·00	3·00	0·4112	0·2161	1·4728	1·0271	0·1413	2·5776
0·20	1·00	4·00	0·5128	0·6735	1·7745	1·0140	0·1432	2·6819
0·20	1·00	6·00	0·6879	2·0480	2·4254	0·9930	0·1597	2·9787
0·20	1·00	8·00	0·8400	3·9677	3·1234	0·9740	0·1847	3·3255

* Asterisk denotes vortex on 'wrong' side.

TABLE—(contd.)

Camber p	Blowing strength c	L	Incidence a	Drag D	Total circulation TC	Position and strength of vortex y/s	z/s	Γ
0·30	0·00	1·00	0·5257	0·0883	0·1716	0·9871	0·0198	0·1565
0·30	0·00	2·00	0·6462	0·3672	0·6307	0·9662	0·0577	0·5339
0·30	0·00	3·00	0·7499	0·8372	1·0906	0·9500	0·0894	0·8797
0·30	0·00	4·00	0·8423	1·4776	1·5416	0·9357	0·1181	1·1972
0·30	0·00	6·00	1·0037	3·2063	2·4108	0·9093	0·1704	1·7621
0·30	0·00	8·00	1·1438	5·4574	3·2395	0·8844	0·2190	2·2521
0·30	0·20	1·00	No solution found					
0·30	0·20	2·00	No solution found					
0·30	0·20	3·00	0·6971	0·6015	1·1062	1·0015	0·0753	1·2813
0·30	0·20	4·00	0·7928	1·1763	1·4799	0·9913	0·0933	1·5167
0·30	0·20	6·00	0·9590	2·7828	2·2966	0·9661	0·1378	2·0163
0·30	0·20	8·00	1·1023	4·9259	3·1208	0·9396	0·1846	2·4911
0·30	0·40	1·00	0·4175	−0·0681	0·6537	1·0355	0·0796	1·4100*
0·30	0·40	2·00	0·5403	0·0835	0·9090	1·0299	0·0791	1·4998
0·30	0·40	3·00	0·6525	0·4366	1·2148	1·0152	0·0893	1·6619
0·30	0·40	4·00	0·7536	0·9758	1·5328	1·0070	0·0992	1·8362
0·30	0·40	6·00	0·9235	2·4868	2·2669	0·9893	0·1313	2·2684
0·30	0·40	8·00	1·0689	4·5307	3·0475	0·9680	0·1704	2·7108
0·30	0·60	1·00	0·3752	−0·1010	0·7255	1·0554	0·0997	1·7995*
0·30	0·60	2·00	0·5045	0·0040	0·9917	1·0362	0·0942	1·8548
0·30	0·60	3·00	0·6146	0·3064	1·2834	1·0268	0·0998	1·9849
0·30	0·60	4·00	0·7158	0·7973	1·5947	1·0183	0·1088	2·1384
0·30	0·60	6·00	0·8912	2·2382	2·2721	1·0031	0·1325	2·5123
0·30	0·60	8·00	1·0389	4·2001	3·0105	0·9860	0·1649	2·9249
0·30	0·80	1·00	0·3360	−0·1151	0·7721	1·0834	0·1203	2·1658*
0·30	0·80	2·00	0·4674	−0·0621	1·0471	1·0500	0·1083	2·1765*
0·30	0·80	3·00	0·5799	0·1985	1·3367	1·0376	0·1102	2·2812
0·30	0·80	4·00	0·6806	0·6408	1·6439	1·0288	0·1178	2·4200
0·30	0·80	6·00	0·8601	2·0117	2·2901	1·0136	0·1366	2·7491
0·30	0·80	8·00	1·0106	3·9053	2·9937	0·9988	0·1638	3·1325
0·30	1·00	1·00	0·3133	−0·0990	0·7688	1·1230	0·1316	2·5018*
0·30	1·00	2·00	0·4311	−0·1168	1·0859	1·0654	0·1224	2·4785*
0·30	1·00	3·00	0·5466	0·1042	1·3766	1·0488	0·1206	2·5592
0·30	1·00	4·00	0·6481	0·5038	1·6796	1·0387	0·1259	2·6826
0·30	1·00	6·00	0·8296	1·8001	2·3115	1·0227	0·1421	2·9799
0·30	1·00	8·00	0·9834	3·6330	2·9878	1·0090	0·1650	3·3352

* Asterisk denotes vortex on 'wrong' side.

TABLE—(contd.)

Camber p	Blowing strength c	L	Incidence a	Drag D	Total circulation TC	Position and strength of vortex y/s	z/s	Γ
0·40	0·00	1·00	No solution found					
0·40	0·00	2·00	0·7814	0·3345	0·4542	0·9839	0·0431	0·4010
0·40	0·00	3·00	0·8901	0·7654	0·8962	0·9741	0·0736	0·7552
0·40	0·00	4·00	0·9867	1·3670	1·3400	0·9655	0·1008	1·0916
0·40	0·00	6·00	1·1536	3·0239	2·2138	0·9488	0·1508	1·7102
0·40	0·00	8·00	1·2958	5·2126	3·0622	0·9312	0·1983	2·2601
0·40	0·20	1·00	0·5976	−0·0263	0·4253	1·0235	0·0449	0·8685
0·40	0·20	2·00	0·7333	0·1714	0·6244	1·0174	0·0445	0·9497
0·40	0·20	3·00	0·8467	0·5466	0·9205	1·0147	0·0550	1·1571
0·40	0·20	4·00	0·9417	1·0626	1·3039	1·0102	0·0744	1·4304
0·40	0·20	6·00	1·1139	2·5899	2·0937	0·9959	0·1142	1·9534
0·40	0·20	8·00	1·2605	4·6612	2·9148	0·9793	0·1575	2·4736
0·40	0·40	1·00	0·5436	−0·1006	0·5951	1·0456	0·0718	1·3938*
0·40	0·40	2·00	0·6861	0·0414	0·7816	1·0312	0·0626	1·4014
0·40	0·40	3·00	0·8060	0·3812	1·0366	1·0263	0·0659	1·5337
0·40	0·40	4·00	0·9081	0·8757	1·3514	1·0232	0·0762	1·7394
0·40	0·40	6·00	1·0798	2·2893	2·0880	1·0138	0·1087	2·2154
0·40	0·40	8·00	1·2295	4·2616	2·8527	1·0015	0·1436	2·6892
0·40	0·60	1·00	0·4940	−0·1336	0·7073	1·0790	0·0974	1·8571*
0·40	0·60	2·00	0·6395	−0·0646	0·8957	1·0461	0·0800	1·7991
0·40	0·60	3·00	0·7648	0·2313	1·1347	1·0373	0·0780	1·8815
0·40	0·60	4·00	0·8724	0·6965	1·4203	1·0330	0·0835	2·0403
0·40	0·60	6·00	1·0485	2·0351	2·1020	1·0256	0·1086	2·4651
0·40	0·60	8·00	1·2004	3·9231	2·8296	1·0157	0·1386	2·9051
0·40	0·80	1·00	No solution found					
0·40	0·80	2·00	0·5938	−0·1467	0·9828	1·0641	0·0975	2·1646*
0·40	0·80	3·00	0·7234	0·0975	1·2140	1·0489	0·0904	2·2065
0·40	0·80	4·00	0·8356	0·5269	1·4845	1·0425	0·0922	2·3295
0·40	0·80	6·00	1·0192	1·8107	2·1209	1·0350	0·1103	2·7017
0·40	0·80	8·00	1·1720	3·6162	2·8239	1·0262	0·1374	3·1166
0·40	1·00	1·00	0·4594	−0·0626	0·6264	1·1588	0·0853	1·5625*
0·40	1·00	2·00	0·5526	−0·1967	1·0418	1·0869	0·1136	2·5046*
0·40	1·00	3·00	0·6825	−0·0182	1·2781	1·0619	0·1031	2·5138
0·40	1·00	4·00	0·7985	0·3697	1·5399	1·0523	0·1015	2·6071
0·40	1·00	6·00	0·9896	1·5985	2·1455	1·0432	0·1139	2·9317
0·40	1·00	8·00	1·1446	3·3325	2·8244	1·0352	0·1378	3·3231

* Asterisk denotes vortex on 'wrong' side.

TABLE—(contd.)

Camber p	Blowing strength c	L	Incidence a	Drag D	Total circulation TC	Position and strength of vortex y/s	z/s	Γ
0·50	0·00	1·00	No solution found					
0·50	0·00	2·00	0·9141	0·3168	0·2546	0·9948	0·0255	0·2345
0·50	0·00	3·00	1·0294	0·7028	0·0339	0·9907	0·0534	0·5798
0·50	0·00	4·00	1·1323	1·2565	1·0767	0·9874	0·0778	0·9226
0·50	0·00	6·00	1·3105	2·8172	1·9265	0·9808	0·1218	1·5779
0·50	0·00	8·00	1·4618	4·9214	2·7721	0·9728	0·1635	2·1860
0·50	0·20	1·00	0·7208	−0·0566	0·3702	1·0267	0·0422	0·8482
0·50	0·20	2·00	0·8609	0·0997	0·5271	1·0202	0·0391	0·8903
0·50	0·20	3·00	0·9833	0·4474	0·7725	1·0192	0·0449	1·0533
0·50	0·20	4·00	1·0926	0·9625	1·0752	1·0193	0·0544	1·2774
0·50	0·20	6·00	1·2766	2·4007	1·8174	1·0162	0·0856	1·8185
0·50	0·20	8·00	1·4327	4·3880	2·6237	1·0086	0·1233	2·3759
0·50	0·40	1·00	0·6620	−0·1580	0·5866	1·0558	0·0727	1·4351*
0·50	0·40	2·00	0·8106	−0·0627	0·7040	1·0354	0·0578	1·3704
0·50	0·40	3·00	0·9382	0·2385	0·9175	1·0307	0·0576	1·4644
0·50	0·40	4·00	1·0510	0·7128	1·1863	1·0294	0·0629	1·6341
0·50	0·40	6·00	1·2453	2·1082	1·8323	1·0286	0·0818	2·0865
0·50	0·40	8·00	1·4044	3·9971	2·5800	1·0248	0·1110	2·5972
0·50	0·60	1·00	No solution found					
0·50	0·60	2·00	0·7600	−0·1899	0·8530	1·0539	0·0769	1·8083*
0·50	0·60	3·00	0·8932	0·0586	1·0375	1·0426	0·0704	1·8382
0·50	0·60	4·00	1·0106	0·4935	1·2839	1·0389	0·0720	1·9634
0·50	0·60	6·00	1·2115	1·8258	1·8813	1·0368	0·0851	2·3490
0·50	0·60	8·00	1·3771	3·6627	2·5695	1·0351	0·1069	2·8155
0·50	0·80	1·00	No solution found					
0·50	0·80	2·00	0·7142	−0·2580	0·9754	1·0809	0·0950	2·2246*
0·50	0·80	3·00	0·8482	−0·0941	1·1446	1·0565	0·0839	2·1931
0·50	0·80	4·00	0·9697	0·2937	1·3698	1·0489	0·0816	2·2753
0·50	0·80	6·00	1·1769	1·5562	1·9322	1·0444	0·0899	2·6028
0·50	0·80	8·00	1·3485	3·3456	2·5815	1·0427	0·1068	3·0294
0·50	1·00	1·00	0·5776	−0·0545	0·5802	1·1836	0·0653	2·6609*
0·50	1·00	2·00	0·7257	−0·1067	0·8960	1·1183	0·0703	2·5613*
0·50	1·00	3·00	0·8047	−0·2100	1·2384	1·0737	0·0975	2·5345
0·50	1·00	4·00	0·9287	0·1161	1·4484	1·0601	0·0917	2·5766
0·50	1·00	6·00	1·1420	1·3013	1·9810	1·0519	0·0955	2·8494
0·50	1·00	8·00	1·3189	3·0368	2·6021	1·0495	0·1089	3·2395

* Asterisk denotes vortex on 'wrong' side.

TABLE—(contd.)

Camber p	Blowing strength c	L	Incidence a	Drag D	Total circulation TC	Position and strength of vortex y/s	z/s	Γ
0·60	0·00	1·00	No solution found					
0·60	0·00	2·00	No solution found					
0·60	0·00	3·00	No solution found					
0·60	0·00	4·00	1·2739	1·1658	0·7692	0·9996	0·0542	0·6888
0·60	0·00	6·00	1·4671	2·6138	1·5668	1·0004	0·0918	1·3470
0·60	0·00	8·00	1·6355	4·6092	2·3815	1·0002	0·1259	1·9859
0·60	0·20	1·00	No solution found					
0·60	0·20	2·00	No solution found					
0·60	0·20	3·00	No solution found					
0·60	0·20	4·00	1·2312	0·8132	0·8718	1·0212	0·0441	1·1261
0·60	0·20	6·00	1·4350	2·2015	1·4988	1·0242	0·0623	1·6086
0·60	0·20	8·00	1·6085	4·1031	2·2283	1·0252	0·0880	2·1629
0·60	0·40	1·00	No solution found					
0·60	0·40	2·00	No solution found					
0·60	0·40	3·00	1·0751	0·1254	0·7077	1·0287	0·0461	1·2952
0·60	0·40	4·00	1·1860	0·4878	0·9712	1·0302	0·0524	1·4838
0·60	0·40	6·00	1·3987	1·8403	1·5875	1·0327	0·0663	1·9207
0·60	0·40	8·00	1·5791	3·7014	2·2443	1·0348	0·0835	2·4082
0·60	0·60	1·00	No solution found					
0·60	0·60	2·00	0·8872	−0·3361	0·7426	1·0519	0·0701	1·7231*
0·60	0·60	3·00	1·0266	−0·1274	0·8134	1·0379	0·0573	1·6468
0·60	0·60	4·00	1·1467	0·2435	1·0583	1·0376	0·0603	1·7974
0·60	0·60	6·00	1·3617	1·4990	1·6605	1·0399	0·0716	2·2041
0·60	0·60	8·00	1·5473	3·3100	2·2911	1·0418	0·0852	2·6519
0·60	0·80	1·00	No solution found					
0·60	0·80	2·00	No solution found					
0·60	0·80	3·00	0·9754	−0·3384	1·0185	1·0561	0·0768	2·1085*
0·60	0·60	4·00	1·1028	−0·0100	1·1572	1·0466	0·0701	2·1175
0·60	0·80	6·00	1·3243	1·1769	1·7235	1·0469	0·0771	2·4697
0·60	0·80	8·00	1·5148	2·9335	2·3372	1·0481	0·0882	2·8856
0·60	1·00	1·00	No solution found					
0·60	1·00	2·00	No solution found					
0·60	1·00	3·00	No solution found					
0·60	1·00	4·00	1·0538	−0.2577	1·3013	1·0598	0·0854	2·4720
0·60	1·00	6·00	1·2864	0·8736	1·7876	1·0542	0·0832	2·7302
0·60	1·00	8·00	1·4818	2·5714	2·3800	1·0542	0·0917	3·1112

* Asterisk denotes vortex on 'wrong' side.

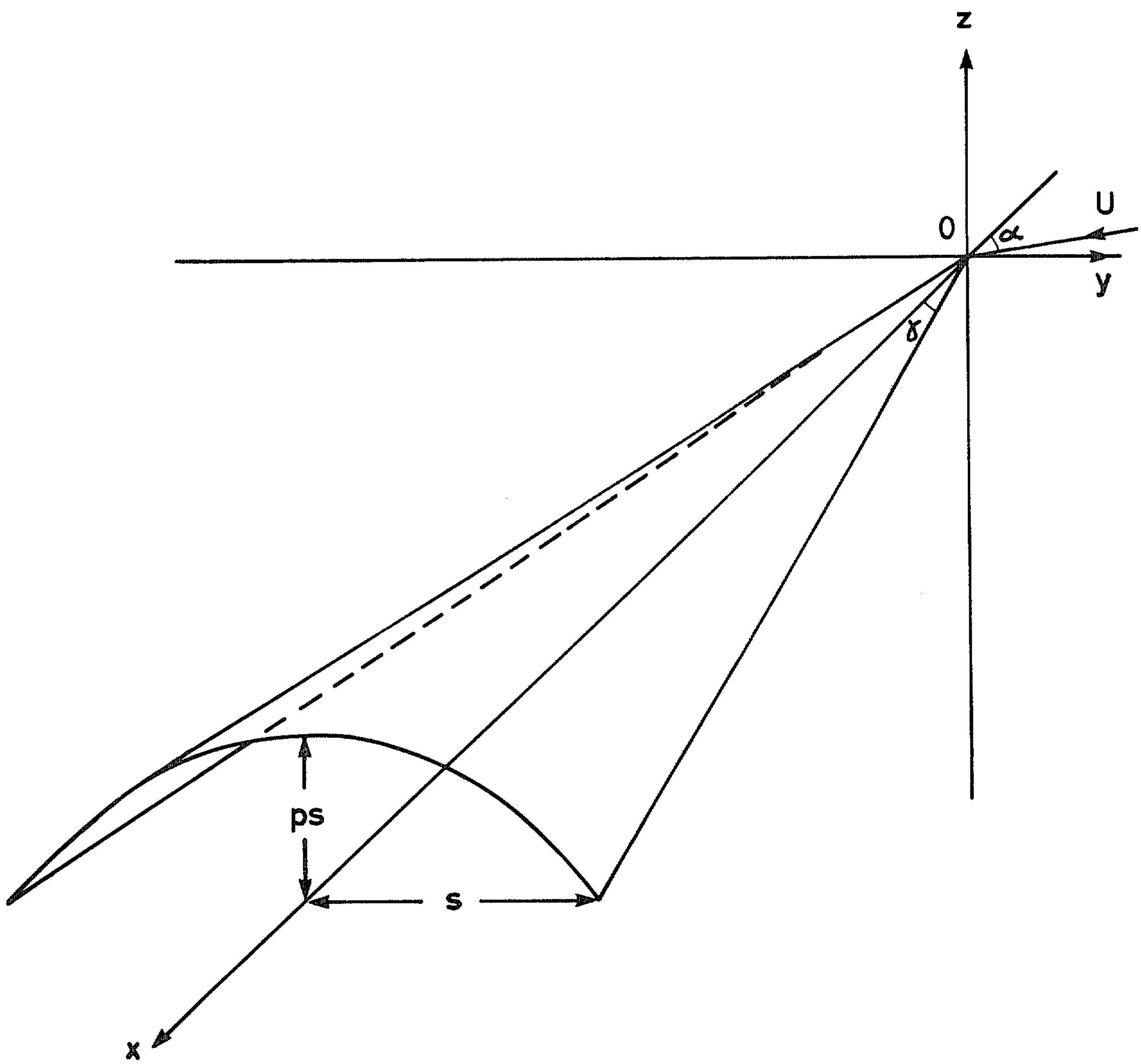

FIG. 1. Wing configuration.

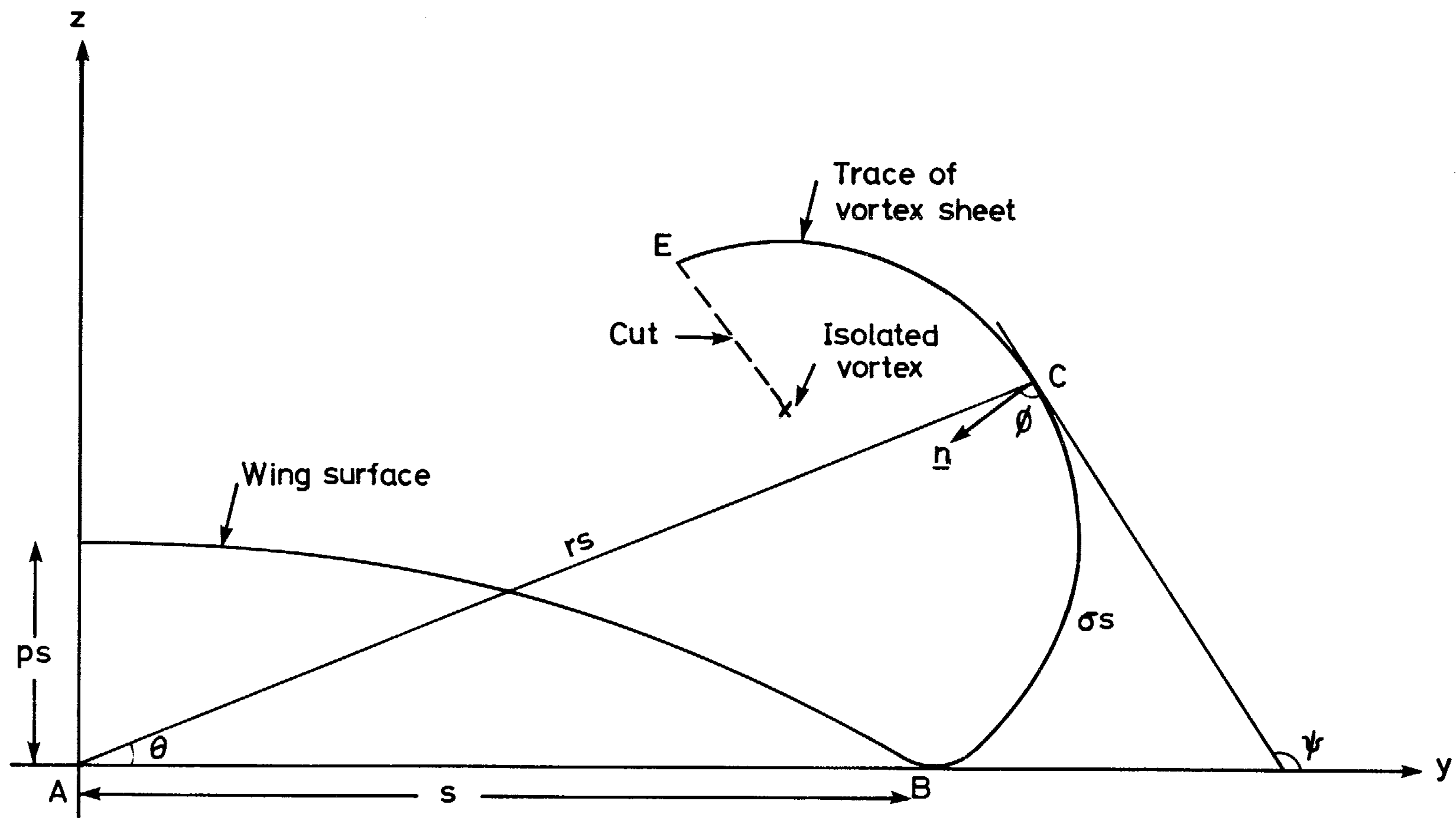

FIG. 2. Axes and coordinates in cross-flow plane.

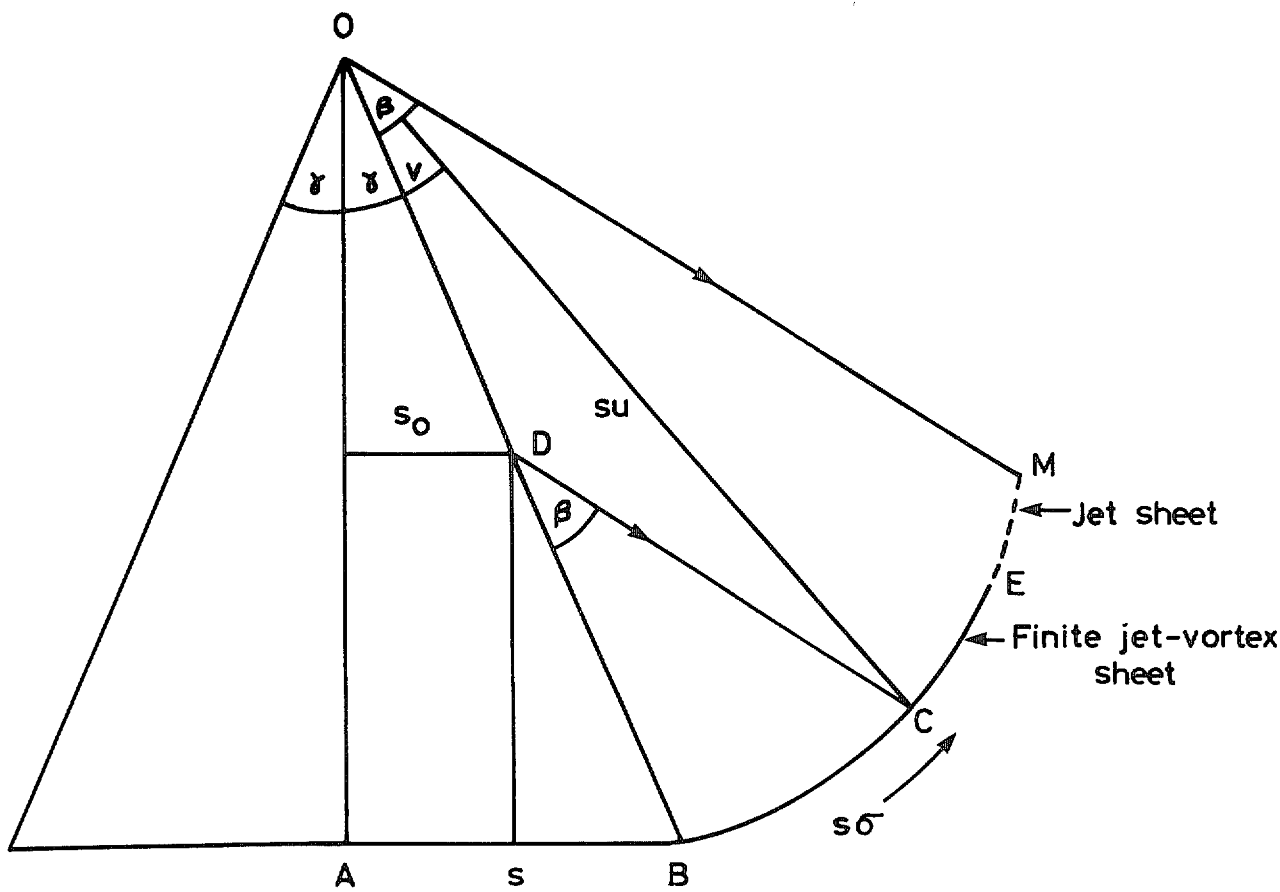

FIG. 3. 'Unrolled' sheet in Oxy plane.

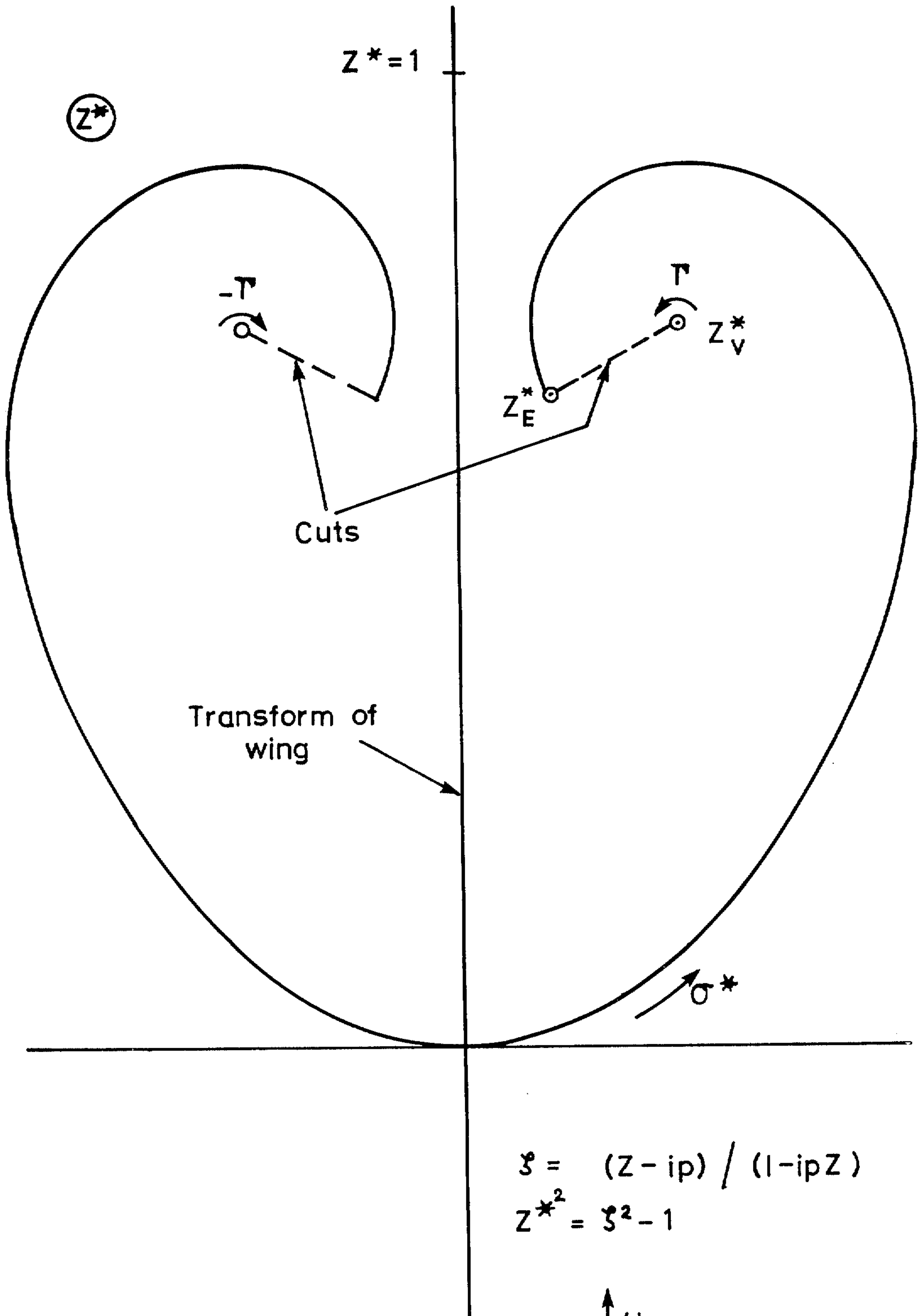

FIG. 4. Configuration in Z^* plane.

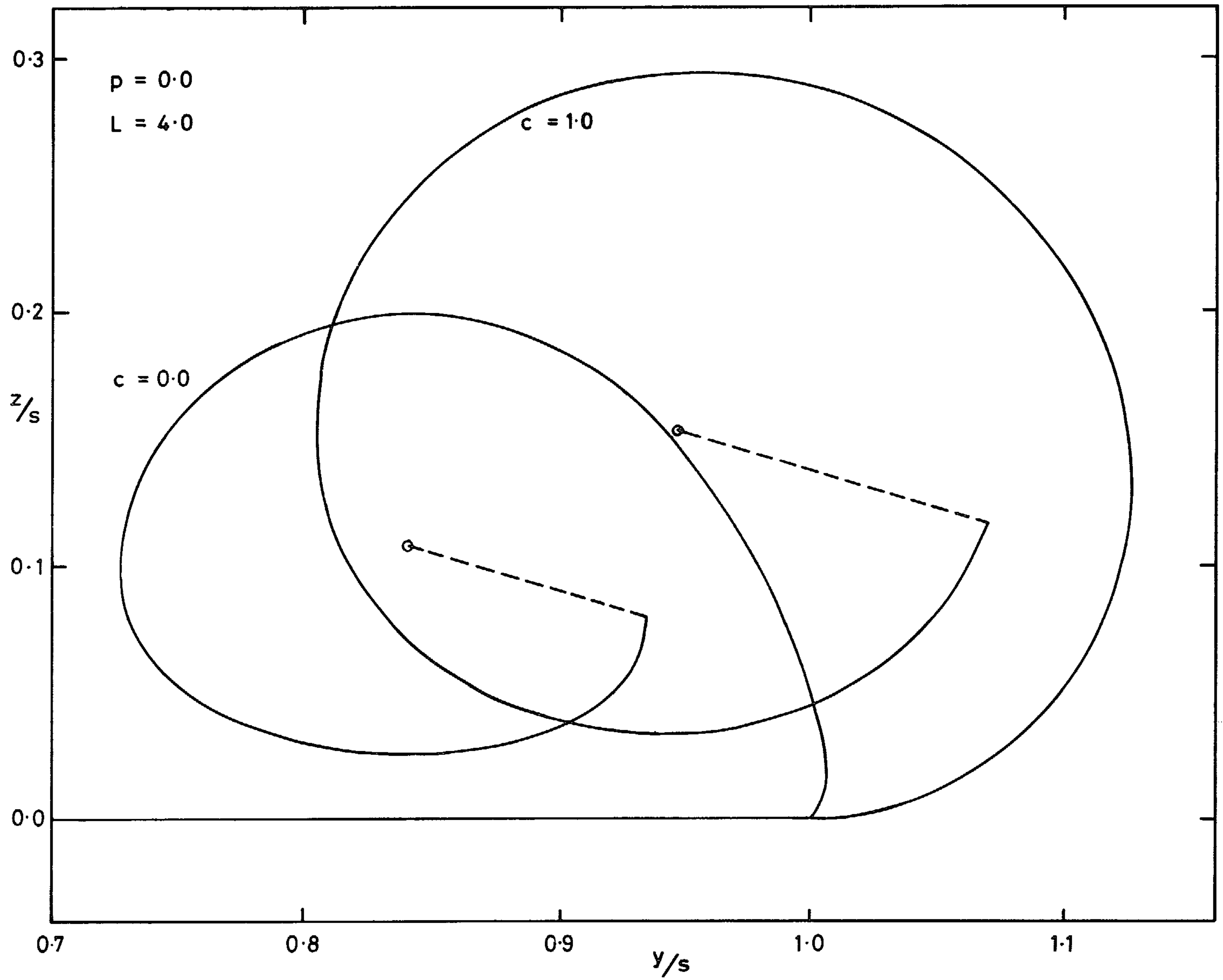

FIG. 5. Sheet shapes $p = 0{\cdot}0$. $L = 4{\cdot}0$. $c = 0{\cdot}0$ and $c = 1{\cdot}0$.

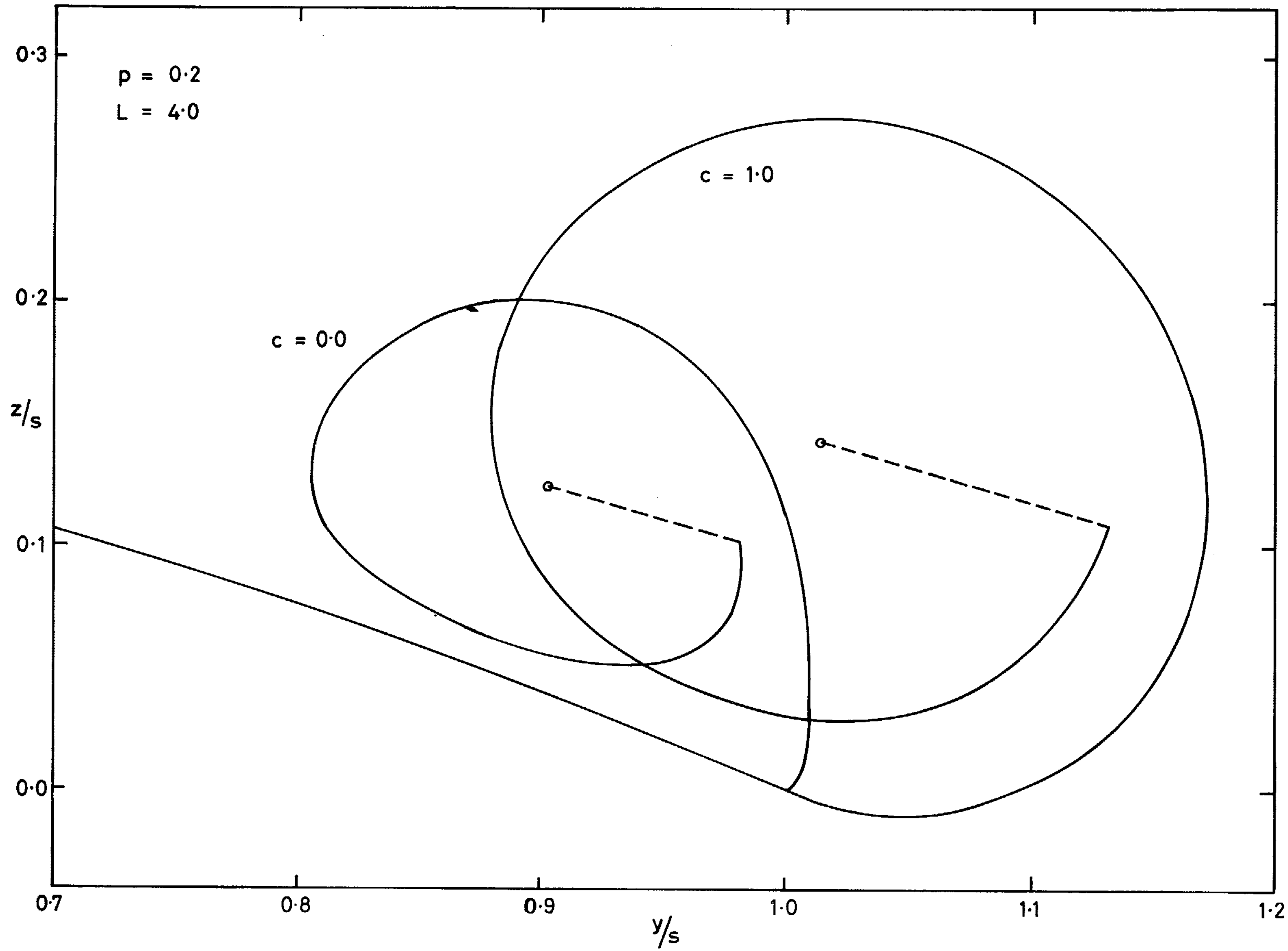

FIG. 6. Sheet shapes. $p = 0{\cdot}2$, $L = 4{\cdot}0$, $c = 0{\cdot}0$ and $c = 1{\cdot}0$.

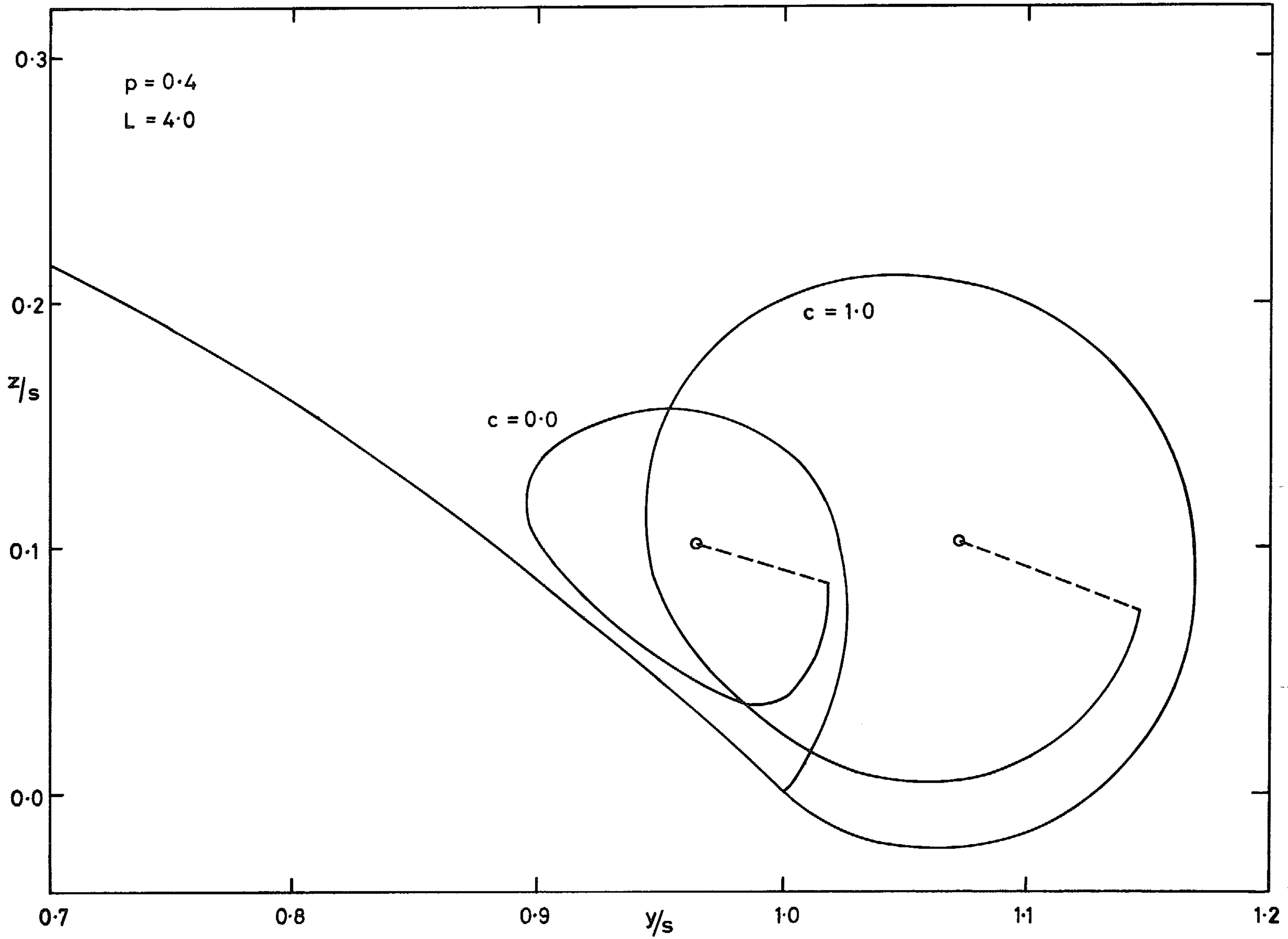

FIG. 7. Sheet shapes. $p = 0{\cdot}4$, $L = 4{\cdot}0$, $c = 0{\cdot}0$ and $c = 1{\cdot}0$.

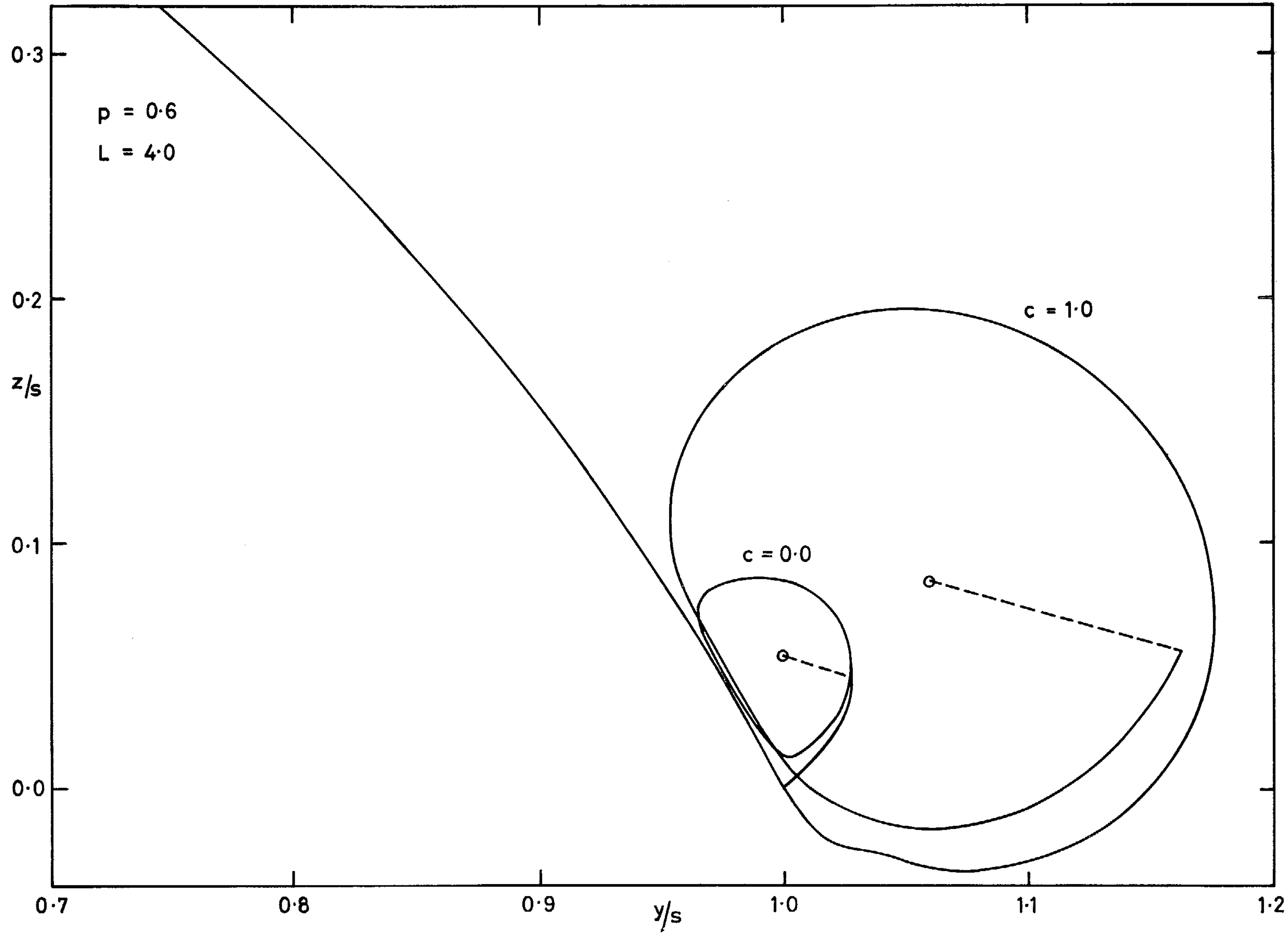

FIG. 8. Sheet shapes. $p = 0{\cdot}6$, $L = 4{\cdot}0$, $c = 0{\cdot}0$ and $c = 1{\cdot}0$.

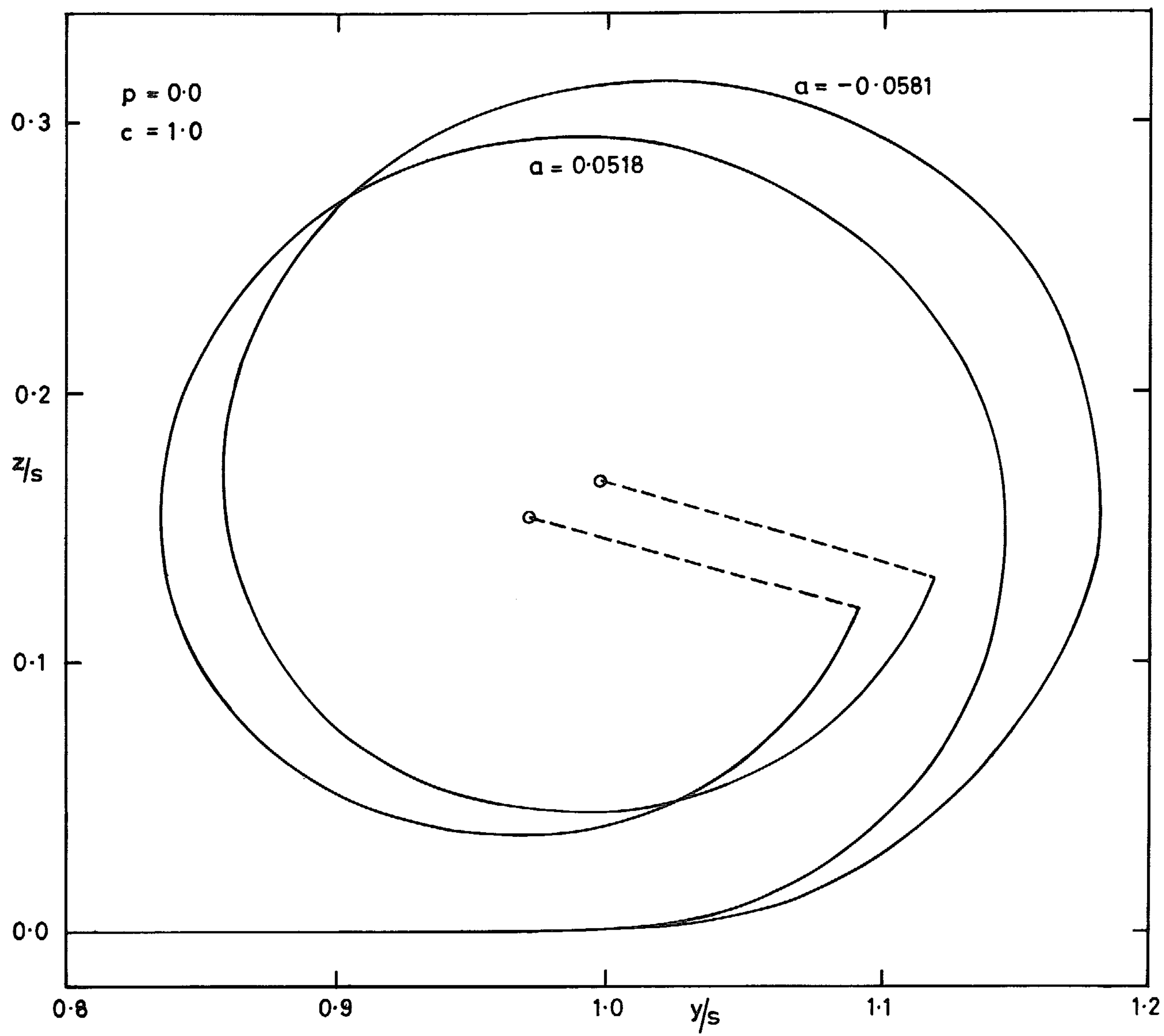

FIG. 9. Comparison of sheet shapes for small incidence with zero camber.

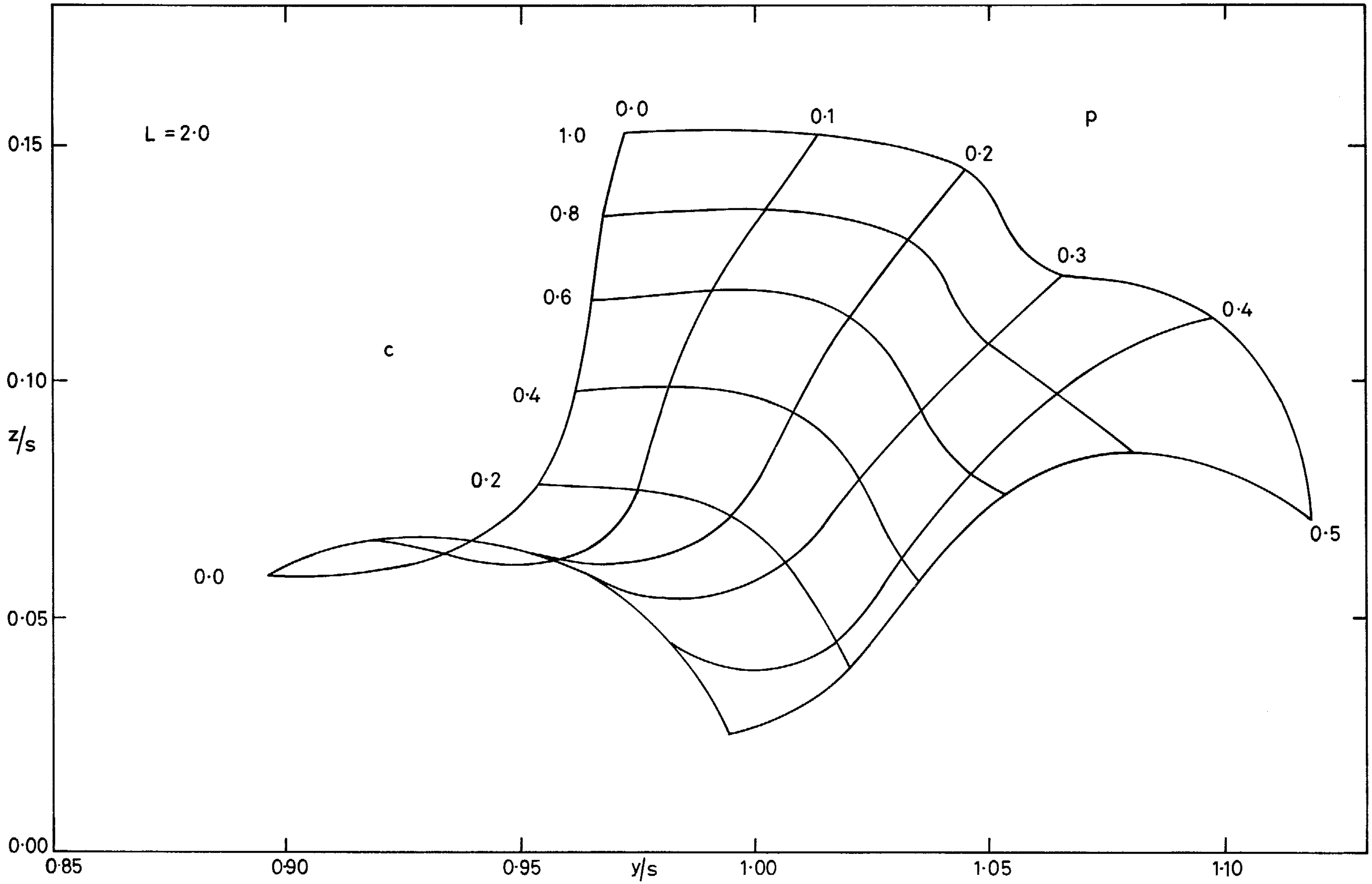

FIG. 10. Vortex positions. $p = 0{\cdot}0(0{\cdot}1)0{\cdot}6$, $L = 2{\cdot}0$, $c = 0{\cdot}0(0{\cdot}2)1{\cdot}0$.

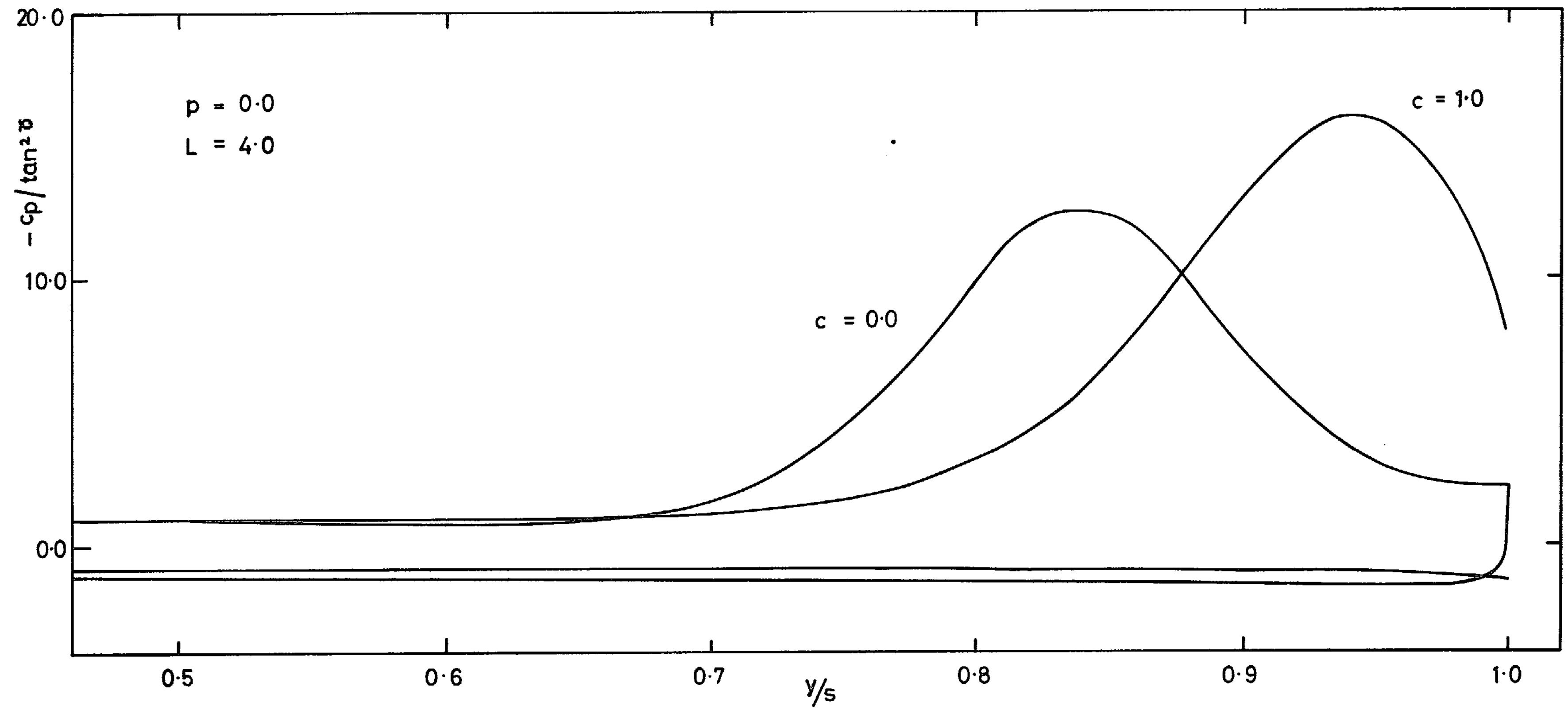

FIG. 11. Wing surface pressures. $p = 0{\cdot}0$, $L = 4{\cdot}0$, $c = 0{\cdot}0$ and $c = 1{\cdot}0$.

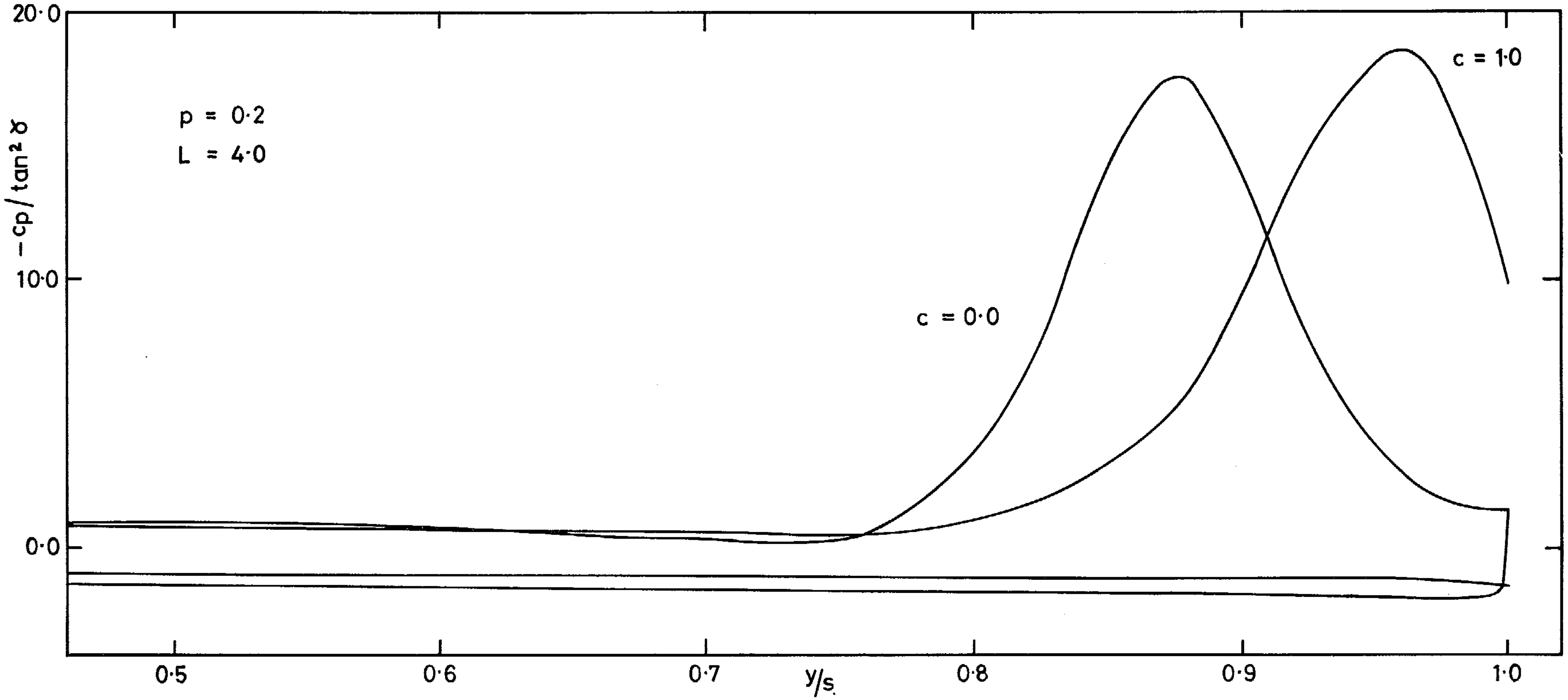

FIG. 12. Wing surface pressures. $p = 0{\cdot}2, L = 4{\cdot}0, c = 0{\cdot}0$ and $c = 1{\cdot}0$.

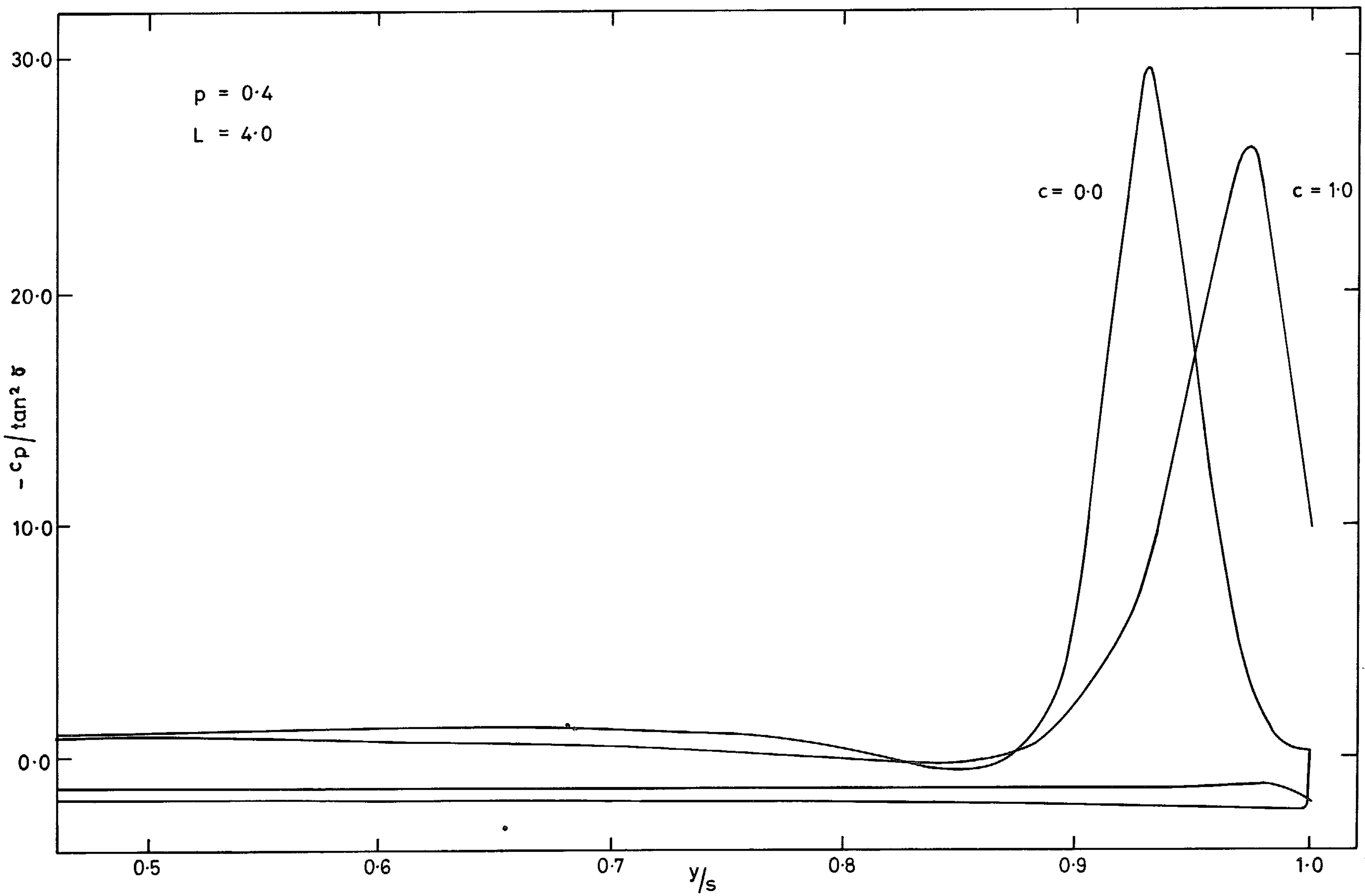

FIG. 13. Wing surface pressures. $p = 0{\cdot}4$, $L = 4{\cdot}0$, $c = 0{\cdot}0$ and $c = 1{\cdot}0$.

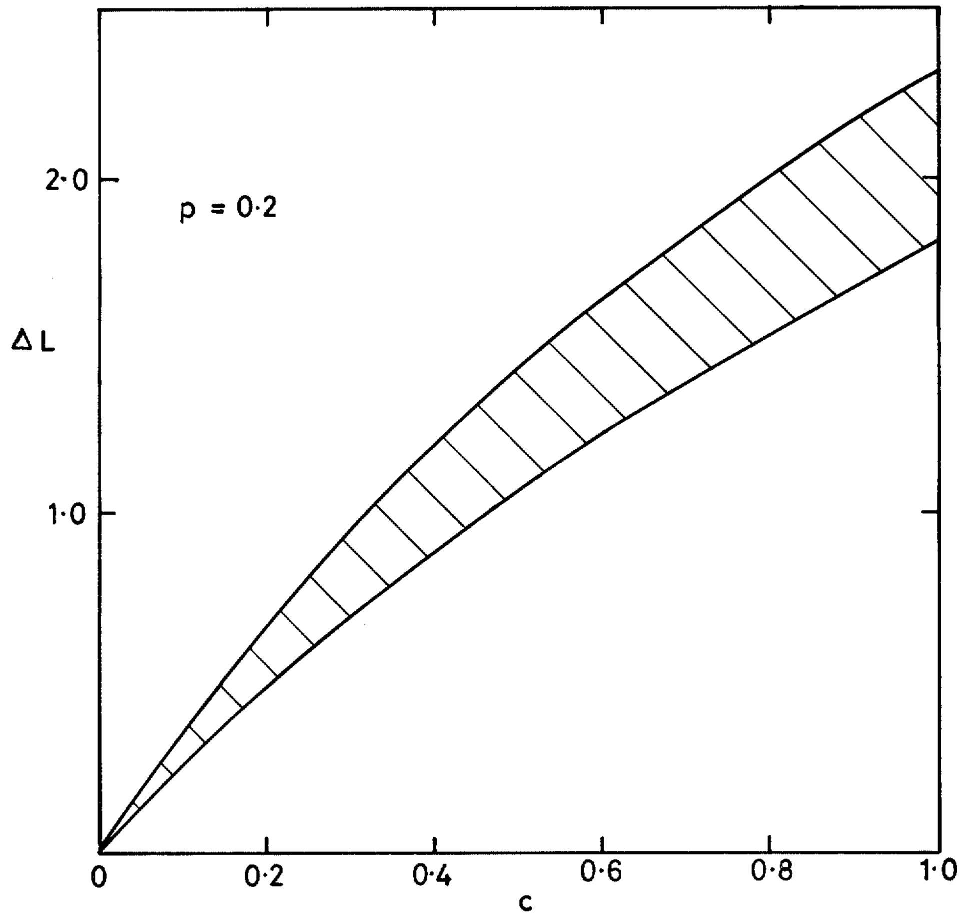

FIG. 14. Variation of ΔL with c for various L_0 with $p = 0{\cdot}2$.

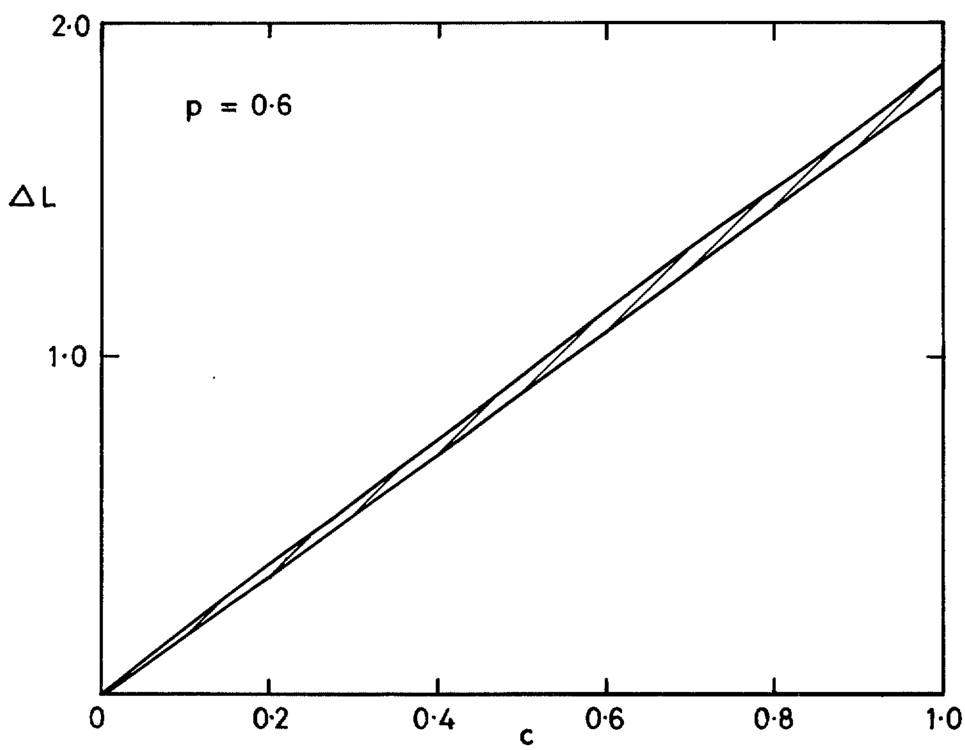

FIG. 15. Variation of ΔL with c for various L_0 with $p = 0{\cdot}6$.

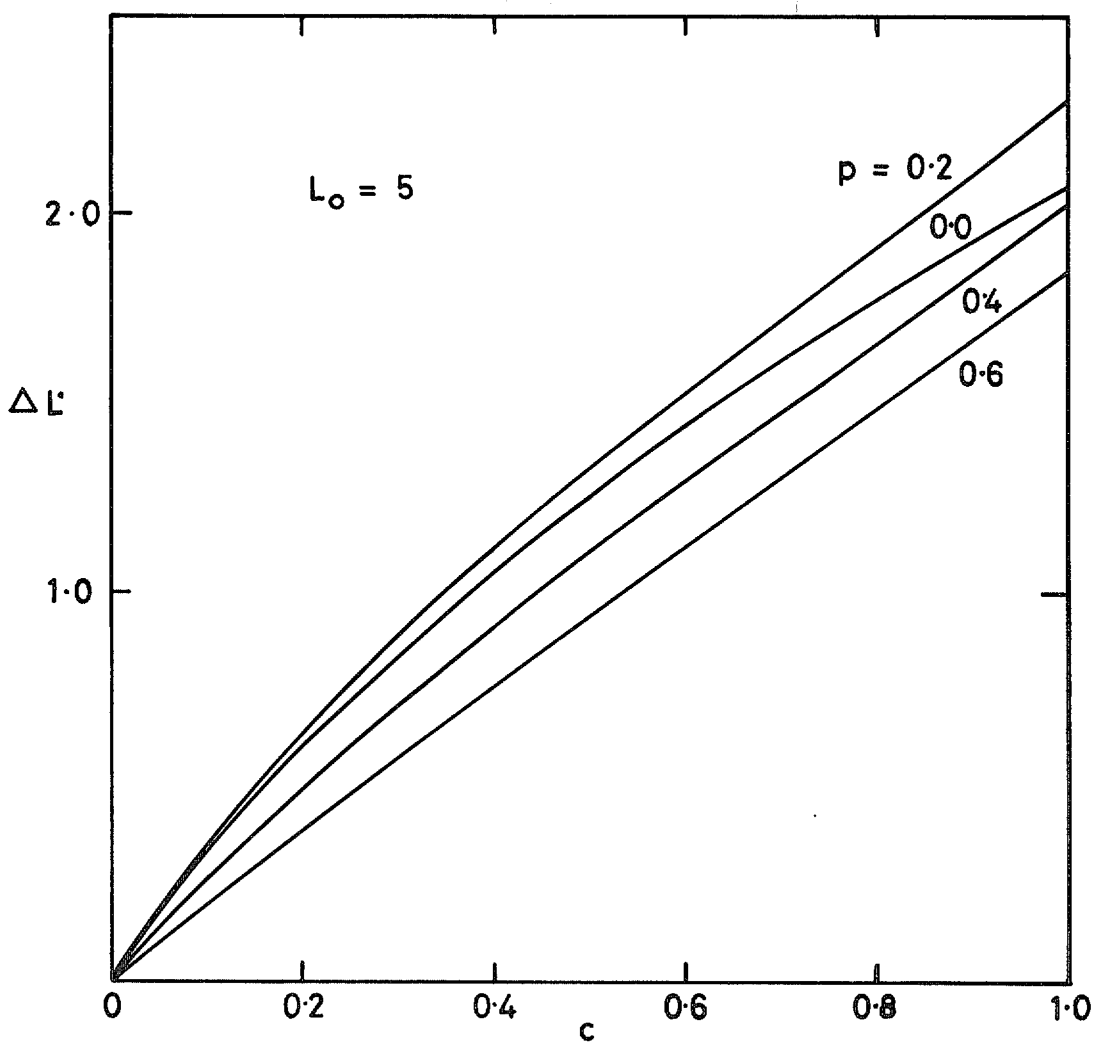

FIG. 16. Variation of ΔL with c for various p with $L_0 = 5$.

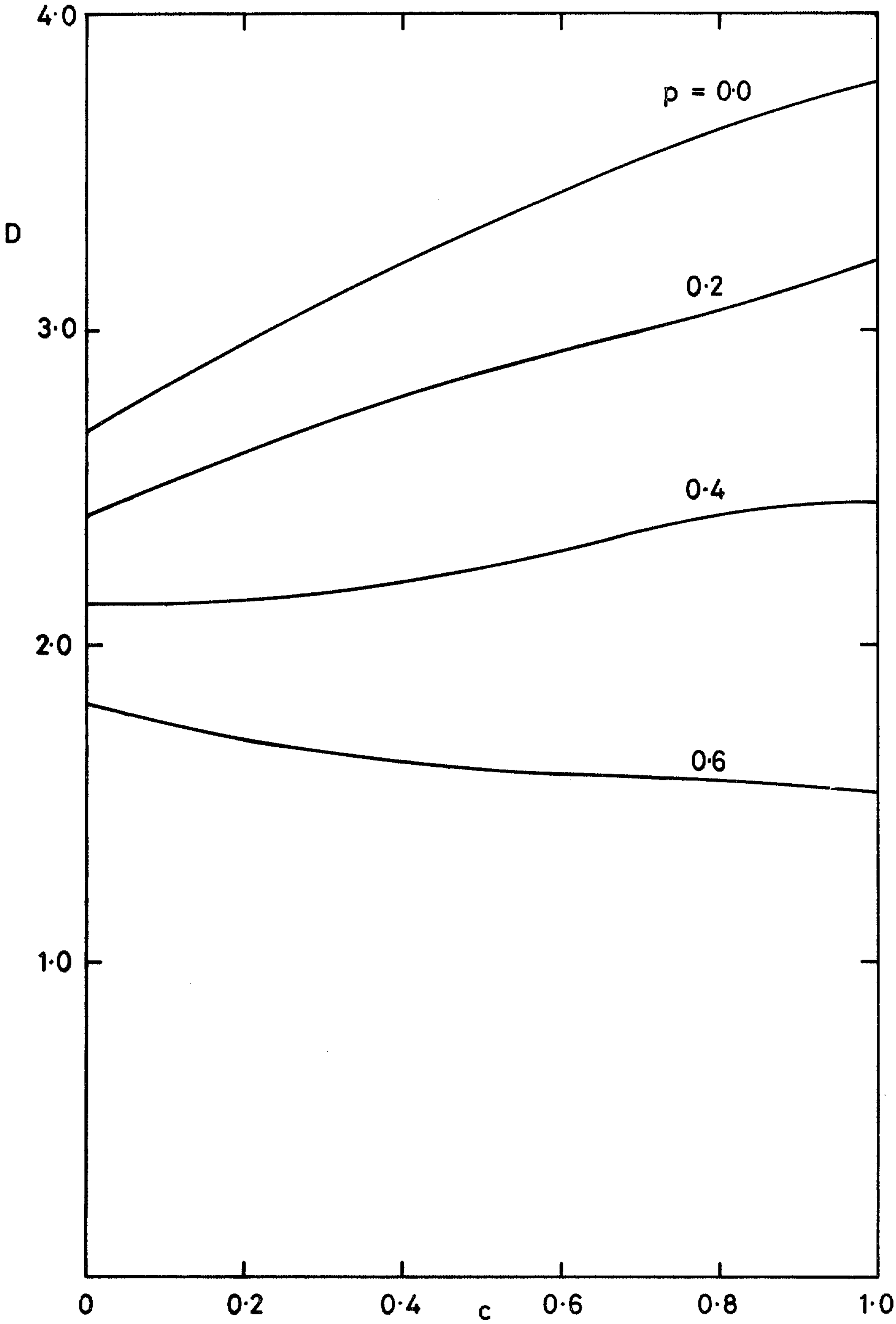

FIG. 17. Variation of the drag parameter with c for various p.

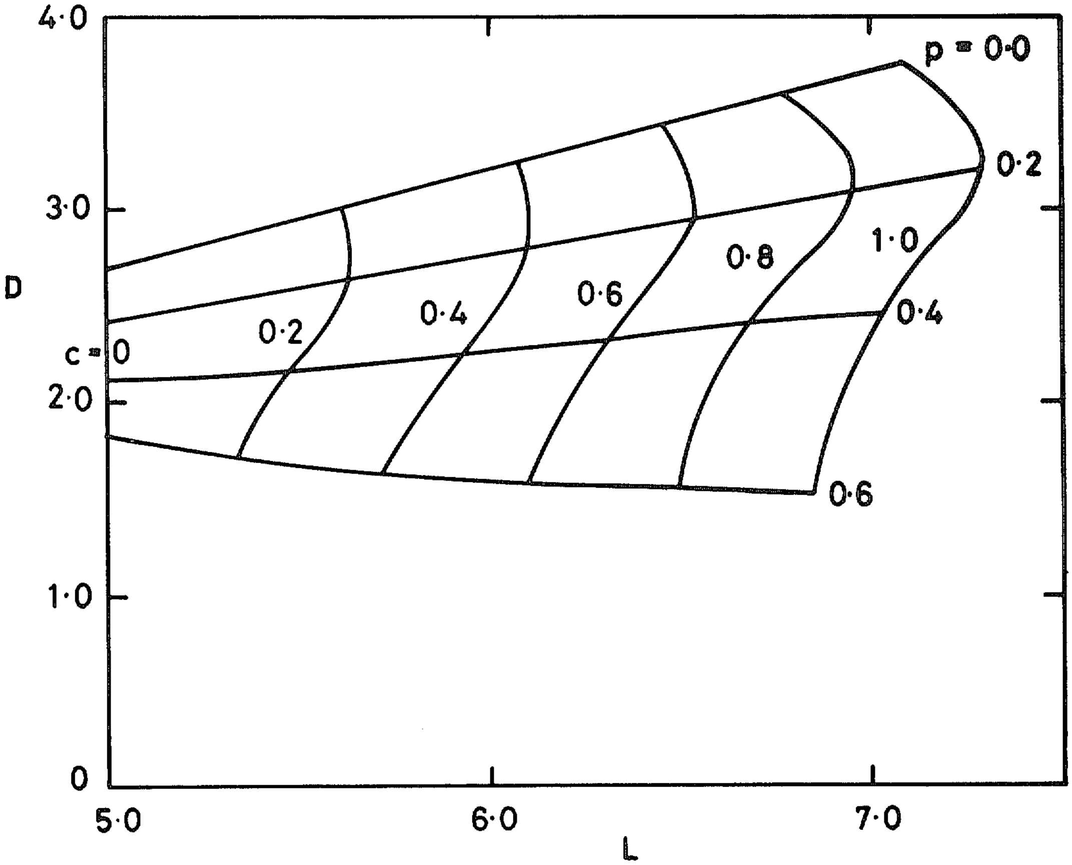

FIG. 18. Variation of the drag with lift for various p and c.

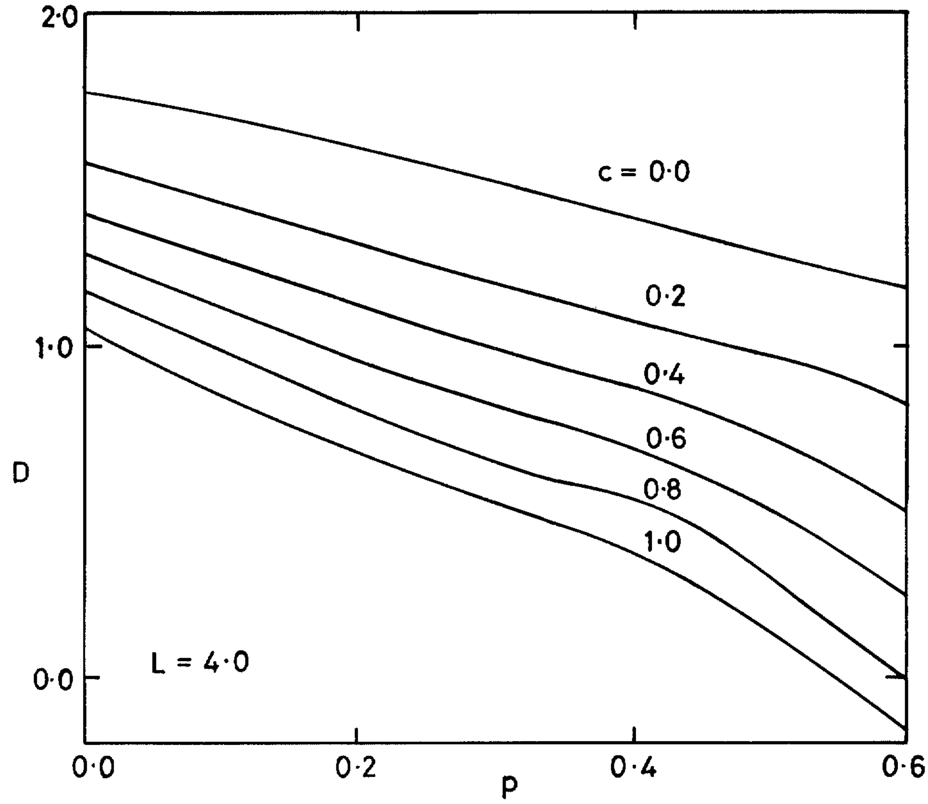

FIG. 19. Variation of drag with camber. $L = 4{\cdot}0, c = 0{\cdot}0(0{\cdot}2)1{\cdot}0$.

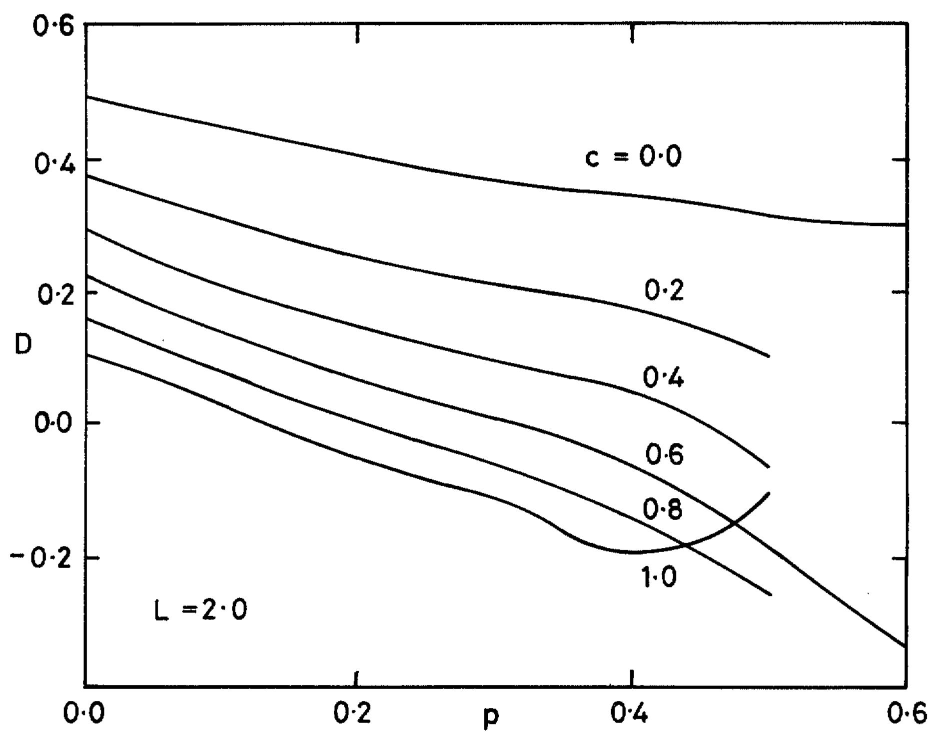

FIG. 20. Variation of drag with camber. $L = 2{\cdot}0, c = 0{\cdot}0(0{\cdot}2)1{\cdot}0$.

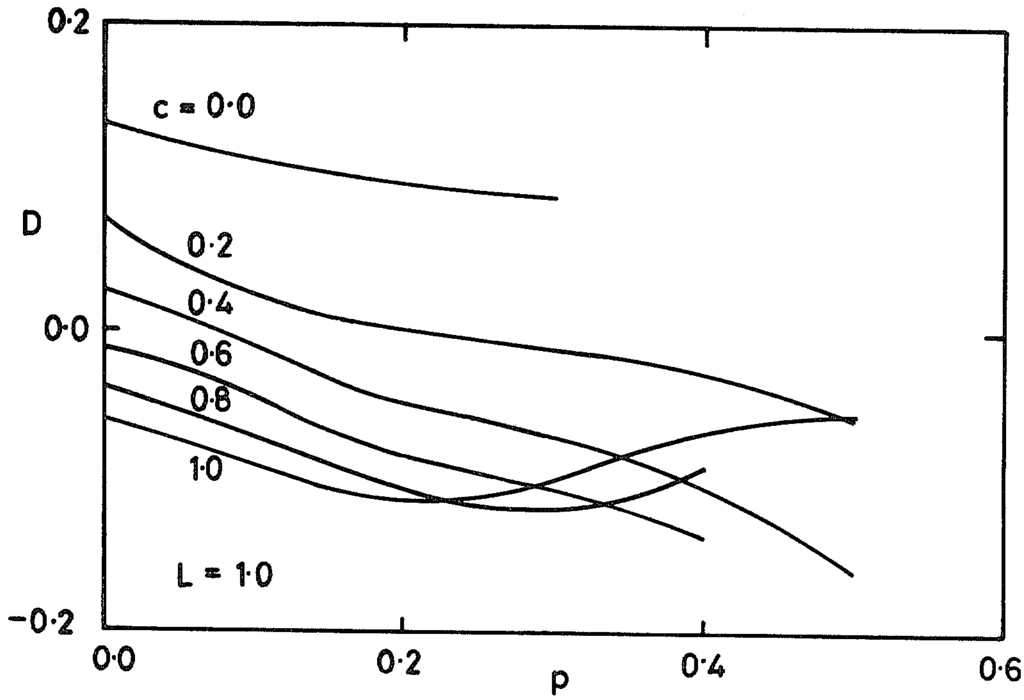

FIG. 21. Variation of drag with camber. $L = 1{\cdot}0$, $c = 0{\cdot}0(0{\cdot}2)1{\cdot}0$.

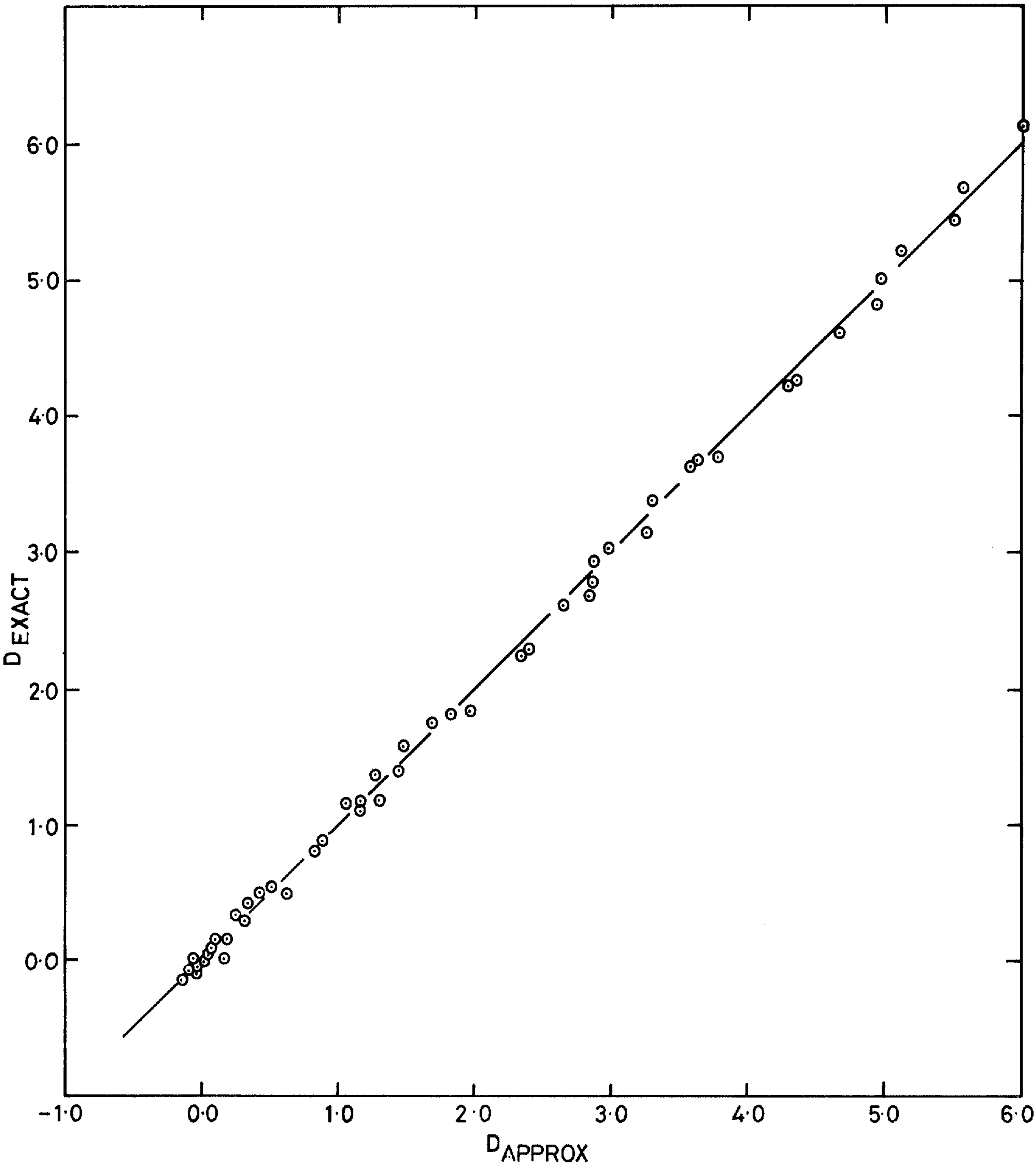

FIG. 22. Comparison of D_{exact} with D_{approx}.

Printed in England for Her Majesty's Stationery Office by J. W. Arrowsmith Ltd., Bristol BS3 2NT
Dd. 587484 K.5. 12/77.

First published 1978

HER MAJESTY'S STATIONERY OFFICE

Government Bookshops

49 High Holborn, London WC1V 6HB
13a Castle Street, Edinburgh EH2 3AR
41 The Hayes, Cardiff CF1 1JW
Brazennose Street, Manchester M60 8AS
Southey House, Wine Street, Bristol BS1 2BQ
258 Broad Street, Birmingham B1 2HE
80 Chichester Street, Belfast BT1 4JY

Government publications are also available through booksellers

R. & M. No. 3
ISBN 0 11 47097